frontiers | Frontiers in Marine Science

TYPE Original Research
PUBLISHED 02 April 2024
DOI 10.3389/fmars.2024.1324436

OPEN ACCESS

EDITED BY
Johan Schijf,
University of Maryland, College Park,
United States

REVIEWED BY
Matthew Jones,
United States Geological Survey (USGS),
United States
N. J. De Winter,
VU Amsterdam, Netherlands
Linda Ivany,
Syracuse University, United States

*CORRESPONDENCE
Shunta Ichimura
ichimura.shunta.a4@s.mail.nagoya-u.ac.jp

RECEIVED 19 October 2023
ACCEPTED 13 March 2024
PUBLISHED 02 April 2024

CITATION
Ichimura S, Takayanagi H, Iryu Y, Takahashi S and Oji T (2024) Shallow-water temperature seasonality in the middle Cretaceous mid-latitude northwestern Pacific.
Front. Mar. Sci. 11:1324436.
doi: 10.3389/fmars.2024.1324436

Shallow-water temperature seasonality in the middle Cretaceous mid-latitude northwestern Pacific

Shunta Ichimura[1]*, Hideko Takayanagi[2,3], Yasufumi Iryu[2,3], Satoshi Takahashi[1] and Tatsuo Oji[4]

[1]Graduate School of Environmental Studies, Nagoya University, Nagoya, Japan, [2]Department of Earth Science, Graduate School of Science, Tohoku University, Sendai, Japan, [3]Advanced Institute for Marine Ecosystem Change (WPI-AIMEC), Tohoku University, Sendai, Japan, [4]Nagoya University Museum (NUM), Nagoya University, Nagoya, Japan

Temperature seasonality during the middle Cretaceous provides vital information about climate dynamics and ecological traits of organisms under the conditions of the "supergreenhouse" Earth. However, sub-annual scale paleotemperature records in the mid-latitude region remain limited. In this study, sclerochronological and stable oxygen isotope ($\delta^{18}O$) analyses of bivalve fossils from the northwestern Pacific (paleolatitude: 44°N) were used to estimate their life history and sub-annual scale temperature patterns of the middle Cretaceous. The materials studied included *Cucullaea* (*Idonearca*) *delicatostriata* and *Aphrodina pseudoplana* recovered from middle Turonian (middle Cretaceous) shallow marine deposits in Hokkaido, northern Japan. Growth increment width and shell $\delta^{18}O$ of *C.* (*I.*) *delicatostriata* revealed that the growth rate was temporally maximized and then minimized, which can be interpreted as representing spring and winter growth, respectively. Approximately 25 fortnightly growth increments occurred within that cycle, suggesting that shell formation proceeded continuously throughout the year. Based on shell $\delta^{18}O$ values, shallow-water temperatures from 28°C to 35°C with 7°C seasonality were estimated, under the assumption that seawater $\delta^{18}O$ values were annually invariant at –1‰ relative to VSMOW. This temperature seasonality in the middle Cretaceous is more than 5°C smaller than the seasonality of modern shallow-water environments at the same latitudes. These findings, taken together with previous studies of other oceanic regions, suggest that the Northern Hemisphere had low seasonal shallow-water temperature variation of up to 10°C in the middle Cretaceous.

KEYWORDS

bivalve, middle Turonian, oxygen isotope, sclerochronology, Yezo Group

1 Introduction

The middle Cretaceous "supergreenhouse" period (Aptian–Santonian; 125–83 Ma; Huber et al., 2018; Petrizzo et al., 2022) is characterized by a warm global climate (Vandermark et al., 2007; Hay, 2008); high pCO_2 levels reaching approximately 1,000 ppm (Foster et al., 2017), nearly approximating the IPCC 6th Assessment Report SSP3-7.0-lowNTCF scenario (Meinshausen et al., 2020); an absence of polar ice sheets (Moriya et al., 2007; MacLeod et al., 2013); and a much flatter equator-to-pole temperature gradient than today (Barron, 1983; Huber et al., 1995; Pucéat et al., 2007). This warm middle Cretaceous period is also associated with drastic faunal and floral transitions (Vermeij, 1977; Lidgard and Crane, 1988). Based on these characteristics, the middle Cretaceous period provides insights into a high-pCO_2 Earth, such as a possible future with accelerated anthropogenic CO_2 emissions. To properly characterize climate in the middle Cretaceous supergreenhouse period, seasonal-scale paleoenvironmental reconstruction is crucial because aspects of climate dynamics, ecology, and evolution of organisms have been controlled by seasonality throughout Earth's history (Denton et al., 2005; Marshall and Burgess, 2015).

Fossil bivalve shells are commonly used to reconstruct sub-annual scale climatic fluctuations over geological timescales (Ivany, 2012; Walliser et al., 2015; Posenato et al., 2022). Stable oxygen isotope ratios ($\delta^{18}O$ values) of marine bivalve shell carbonates (mainly aragonite and calcite) can be used for seawater temperature reconstruction because bivalve shells are precipitated in oxygen isotope equilibrium with ambient seawater (Epstein et al., 1953; Grossman and Ku, 1986). Bivalves form disconformities and translucent bands within their shells (called growth lines) when their shell growth stops or slows due to cyclic or irregular environmental or physiological changes (Kennish and Olsson, 1975; Ohno, 1989; Schöne et al., 2003). Furthermore, annual shell growth rates of bivalves ontogenetically decrease due to reductions in daily growth rates (Jones and Quitmyer, 1996), which are mainly observed in regions with small seasonality (Schöne et al., 2005; Reza Mirzaei et al., 2017) and increases in growth cessation interval, which can be observed worldwide (Hall et al., 1974; Tanabe, 1988; Jones et al., 1989; Tanabe et al., 2017, 2020). The timing of shell formation, temporal shell growth rate, and age of bivalves can be estimated by identifying the timing of growth line formation on shells and measuring the widths and numbers of these lines (Jones, 1983; Sato, 1997; Kubota et al., 2017).

Fossil bivalves with primary low-Mg calcite shells have often been used for climate reconstruction in deep time (Beard et al., 2015; de Winter et al., 2017, 2021) because low-Mg calcite is less susceptible to diagenetic alteration than aragonite. For example, $\delta^{18}O$ values of rudists with large, thick, and low-Mg calcite shells have been preferentially used for seasonal-scale paleotemperature reconstruction in the middle Cretaceous paleoenvironmental studies (Steuber et al., 2005; Walliser and Schöne, 2020; Schmitt et al., 2022). However, because rudists were reef/bioherm builders that primarily inhabited low-latitude shallow oceans, seasonal-resolution sea surface temperature (SST) records for the middle Cretaceous have mostly been reported from the low-latitude Tethys Ocean (Steuber et al., 2005; Walliser and Schöne, 2020; Huck and Heimhofer, 2021). Because seasonality varies with latitude, SST seasonality must be investigated at low latitudes, as well as middle and high latitudes, to elucidate its global seasonal climatic trends. Furthermore, the mid-latitude region is the best area for identifying maximal seasonal temperature fluctuations (Ivany, 2012; Ivany and Judd, 2022). Despite its importance, however, few middle Cretaceous studies have included reconstruction of paleo-seawater temperature and its seasonality from carbonate fossil shells in mid-latitude regions. On the other hand, aragonitic shells produced by mollusks with sufficient thickness for sclerochronological and geochemical analyses from shell cross sections (e.g., *Aphrodina*, *Cucullaea*, and *Glycymeris*) were common at low latitudes, as well as middle and high latitudes, during the middle Cretaceous (Ando and Kodama, 1998; Squires, 2010; Hoşgör and Yılmaz, 2019). The sub-annual scale paleoenvironment, including shallow-water temperature, can be reconstructed from aragonitic fossil shells in deep time if evaluation of fossil preservation shows that shell aragonite is well-preserved (Walliser et al., 2015; Hall et al., 2018; Meyer et al., 2018; Posenato et al., 2022).

The Cretaceous Aptian–Maastrichtian Yezo Group in Hokkaido (northern Japan), deposited in the middle latitudes of the northwestern Pacific, contains a variety of well-preserved marine fossils, including ammonites, bivalves, and gastropods (Suzuki et al., 1998; Hikida et al., 2003; Yabumoto et al., 2012). The Yezo Group was mainly deposited in the deep ocean. However, some parts, such as the Mikasa Formation (latest Albian–Turonian), were deposited in a shallow ocean with abundant shallow-water bivalves (Tashiro, 1995; Ando and Kodama, 1998). This study presents detailed sclerochronological and oxygen isotope records of bivalve fossils from the Mikasa Formation to reveal seasonal-scale shallow-water temperature records and their life history.

2 Geological setting

Aptian–Maastrichtian forearc (Yezo Basin) sediments of the paleo-Asian continental eastern margin (Takashima et al., 2004), called the Yezo Group, are widely distributed from Soya to Urakawa areas, central Hokkaido, northern Japan (Figure 1A). Paleomagnetic studies showed that the paleolatitude of the Yezo Basin was approximately 44° N in the Late Cretaceous (Tamaki and Itoh, 2008; Kitagawa et al., 2016). An exception is the Urakawa area, which was at approximately 16.7°N during the Campanian (Late Cretaceous) before being transported to its present position (Tamaki et al., 2008). The Cenomanian–Campanian Yezo Basin was affected by a southward shallow-water current system comparable to the modern Oyashio Current based on neodymium isotope ($^{143}Nd/^{144}Nd$ ratio) analysis of fish bone and tooth fossils from the Yezo Group (Moiroud et al., 2013). The mean annual SST in the middle–late Turonian Yezo Basin has been estimated as 26°C–29°C from planktonic foraminiferal $\delta^{18}O$ data (Moriya, 2011).

The Albian–Turonian Mikasa Formation, the Yezo Group is characterized by sandstone with hummocky cross-stratification (HCS) (Ando, 1987). The Mikasa Formation is distributed across the Sorachi–Ikushunbetsu Anticline (Figure 1B) (Ando, 1990b). The Mikasa Formation has various sedimentological facies that

10.3389/fmars.2024.1324436

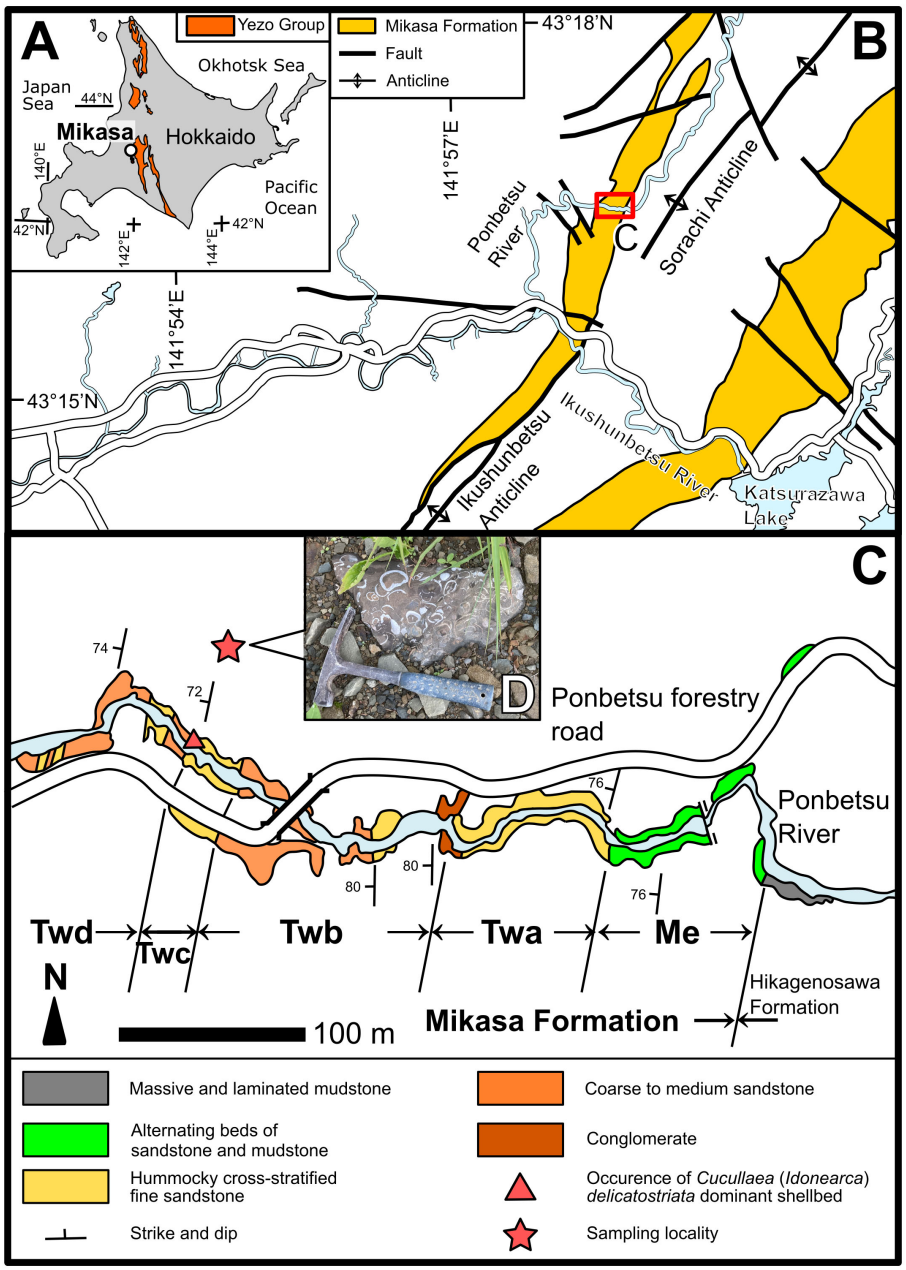

FIGURE 1
Geological map of Hokkaido modified from Takashima et al. (2004) **(A)** and the Mikasa area modified from Kikuchi (2018) **(B)**. **(C)** Map of the Ponbetsu River section modified from Ando and Kodama (1998), and details of the sampling locality. Me, Twa, Twb, Twc, and Twd in **(C)** represent sedimentary units of the Mikasa Formation in the Ponbetsu River section from Ando (1987). **(D)** Photograph of the sampled shellbed.

were deposited from the lagoon to the outer shelf, mainly under shallow-water conditions (Ando, 1990a). The Mikasa Formation is almost continuously exposed along the Ponbetsu River in Ponbetsu-cho, Mikasa City, central Hokkaido (Ponbetsu River section; Ando, 1987) (Figures 1C, 2) and is divided into five units based on sedimentary facies (Matsuno et al., 1963), designated Me (main part of the Middle Yezo Group, unit e), Twa, Twb, Twc, and Twd (Tw denotes the *Trigonia* sandstone in the western wing of the Sorachi–Ikushunbetsu Anticline) (Figures 1C, 2; Yabe, 1926; Matsumoto, 1951; Shimizu et al., 1955; Takashima et al., 2004). The Twc unit is approximately 32 m-thick and consist of fine- to very fine-grained sandstone with hummocky cross-stratification (HCS). This unit is considered to have been deposited from the lower shoreface to the shallow inner shelf, in waters tens of meters deep (Ando and Kodama, 1998). The Twc unit has been correlated with the middle Turonian based on the occurrence of an age-indicative ammonoid *Subprionocyclus neptuni* (Matsumoto, 1965) and inoceramid *Inoceramus hobetsensis* (Ando, 1987). The Twd unit is approximately 100 m-thick and mainly composed of medium- to coarse-grained sandstone with HCS (Ando and Kodama, 1998). The occurrence of *I. hobetsensis* in the lowest part and *I. teshioensis* in the uppermost part of the Twd unit

10.3389/fmars.2024.1324436

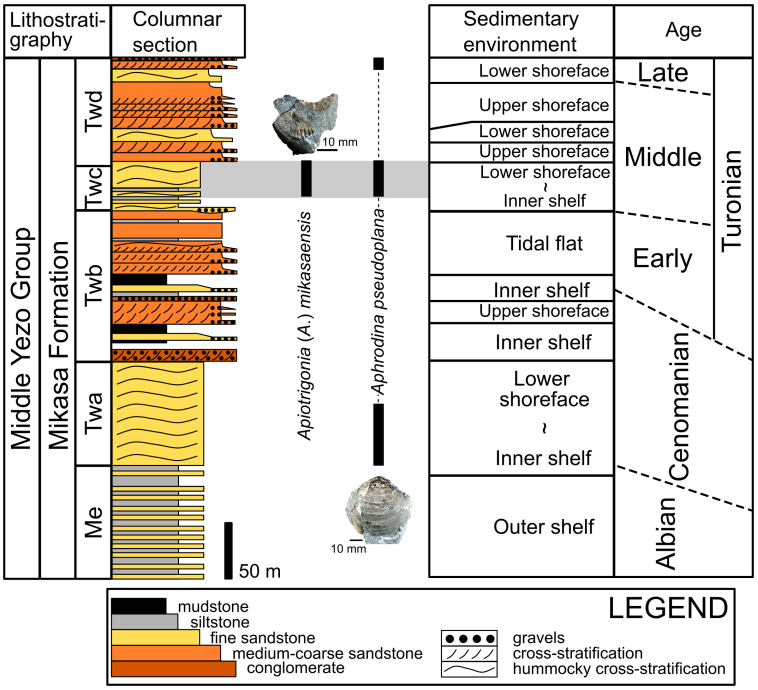

FIGURE 2
Columnar section with sedimentary setting and deposition age of the Mikasa Formation at the Ponbetsu River section modified from Ando (1987, 1990b) and Ando and Kodama (1998). Black bars with photographs of bivalve fossils represent the stratigraphic occurrences of identified bivalves in the studied shellbed according to Ando and Kodama (1998). Gray zones indicate the suggested stratigraphic ranges of our studied materials.

indicates that the Twd unit was deposited in the middle to late Turonian (Ando, 1987).

3 Materials and methods

3.1 Field sampling

A boulder of calcite-cemented fine-grained sandstone containing abundant mollusk fossils (coquina) was collected alongside a forest road near the Ponbetsu River section (Figures 1C, D). In this rock, disarticulated bivalves (*Aphrodina pseudoplana* (Figures 2, 3D), *Apiotrigonia* (*A.*) *mikasaensis* (Figure 2), *Cucullaea* (*Idonearca*) *delicatostriata* (Figures 3A–C), and possibly *Leptosolen* sp.) and gastropods (possibly naticids) were observed. Most fossils from the coquina were identified as *C.* (*I.*) *delicatostriata*, and other species were observed as only one or a few individuals.

Although this coquina was found as an isolated unrooted block, the shellbed was determined to be derived from the Twc unit or the lowermost part of the Twd unit because large boulders of fine-grained sandstone rich in *C.* (*I.*) *delicatostriata* were exclusively found near the outcrop of the Twc unit and lowermost part of the Twd unit in the Ponbetsu River section (Figure 1C); moreover, *Apiotrigonia* (*A.*) *mikasaensis*, a trigoniid bivalve restricted to the Turonian age (Tashiro, 1979), was observed in the collected coquina (Figure 2). In the studied succession, only Twc and Twd units are correlated with the Turonian, and the occurrences of *A.* (*A.*) *mikasaensis* in the Ponbetsu River section were limited to the upper Twc and lower Twd units (Ando and Kodama, 1998). These findings indicated that the studied shellbed originated from Twc or lower Twd units (Figure 2).

3.2 Sample preparation

The surfaces of the bivalve shells were carefully cleaned and exposed from the sandstone matrix. For this study, three shells of *C.* (*I.*) *delicatostriata* (Figures 3A–C; labeled PU-1, PU-2, and PU-5) and one shell of *A. pseudoplana* (Figure 3D) were selected for subsequent growth line observation and geochemical analysis, considering that these species have sufficiently thick shells for observation and geochemical sampling from cross-sections. Additionally, the abundant occurrence of *C.* (*I.*) *delicatostriata* allows intraspecific comparisons, thus improving data reliability. Shell surfaces were coated with epoxy resin to avoid mechanical damage during preparation. Shells were diagonally cut along their maximum growth direction using a diamond saw (Figures 4A, B). One side was polished with silicon carbide up to #3,000 (Figures 4A, B). Regarding *C.* (*I.*) *delicatostriata*, the other side of the cross-section was used to make a thin section (0.1 mm thickness) for growth line observation. Small pieces of shells were collected from the studied shells to evaluate the extent of diagenetic alteration and determine the diagenetic level according to preservation index (PI) (Cochran et al., 2010; Knoll et al., 2016) via scanning electron microscopy (SEM) (Figures 4A, B). The polished shell surface was etched with 5% acetic acid for 15 min prior to microstructure observation with SEM.

10.3389/fmars.2024.1324436

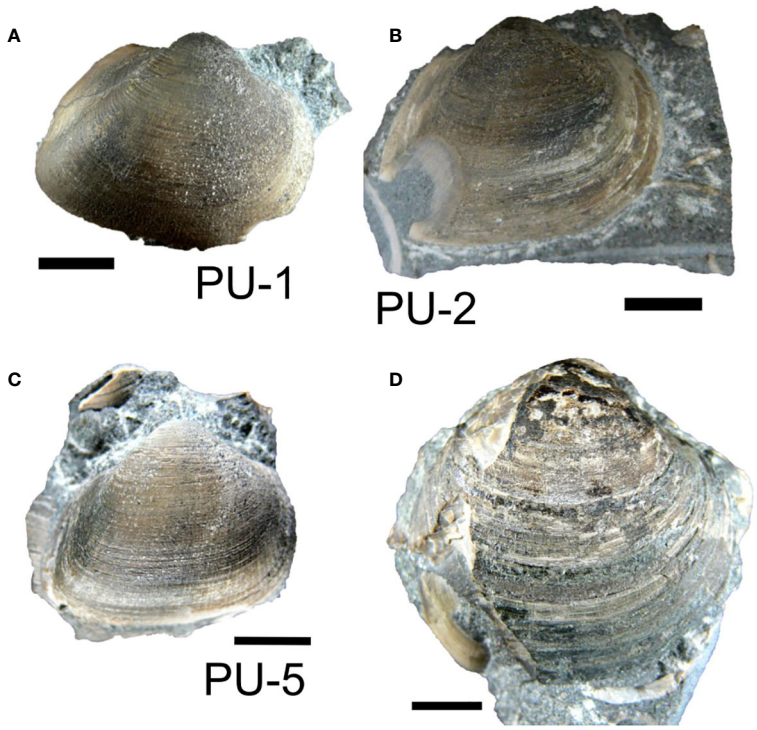

FIGURE 3
Photographs of the *Cucullaea* (*Idonearca*) *delicatostriata* (**A**: PU-1, **B**: PU-2, **C**: PU-5) and *Aphrodina pseudoplana* **(D)** shells used in this study. Scale bar = 10 mm.

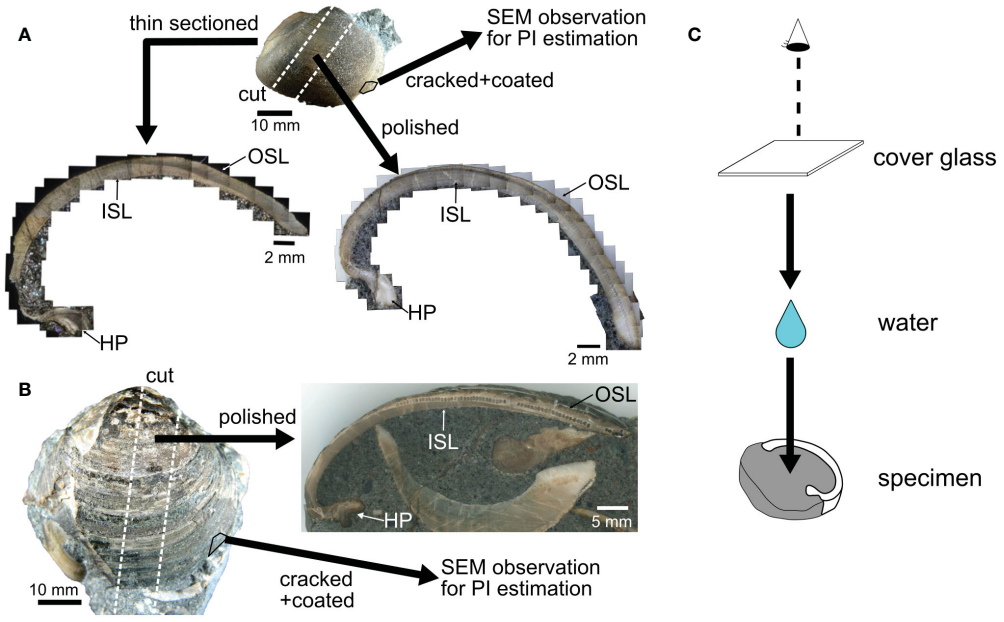

FIGURE 4
Sample preparation of *Cucullaea* (*Idonearca*) *delicatostriata* **(A)** and *Aphrodina pseudoplana* **(B)** shells. The valves were cut perpendicular to the maximum growth direction. One side of the cutting slab was polished to make a polished slab and the other side of each *C.* (*I.*) *delicatostriata* shell was thin-sectioned. Small fragments of shell were sampled by cracking each shell and then coating the cracked surface with platinum. The coated shell was used for preservation state estimation based on the PI scale (Cochran et al., 2010; Knoll et al., 2016). The surfaces of the thin section and polished shell were wetted and covered with cover glass during observation **(C)**. Small holes in the polished sections are the remains of samples used for stable isotope analysis. OSL, outer shell layer; ISL, inner shell layer; HP, hinge plate.

3.3 Evaluation of the extent of diagenetic alteration

Evaluation of diagenetic effects on shell microstructure and mineralogy is essential for reliable paleoenvironmental reconstruction because diagenesis alters the original chemical composition of the shell (Cochran et al., 2010; Pederson et al., 2019). Shell microstructure and mineralogy of the studied shells were analyzed to determine the extent of diagenetic alteration. Thin sections and polished sections of the shells were carefully observed with a binocular microscope and a petrographic microscope to identify macro-scale diagenetic products, such as mosaic calcite crystals (Maliva et al., 2000; Pederson et al., 2019).

3.3.1 Raman spectroscopic analysis

Raman spectroscopic analysis was conducted to identify the mineral composition of the studied fossils using a confocal Raman micro-spectrometer (Nicolet Almega XR; Thermo Fisher Scientific, Bremen, Germany) in the Petrology and Mineralogy Laboratory of Nagoya University, Nagoya, Japan. A 532 nm Nd-YAG laser at a power of approximately 10 mW was irradiated to the thin sections and the polished sections of studied shells through a confocal microscope (BX51; Olympus, Tokyo, Japan) with a 100× objective (Olympus Mplan-BD 100X; numerical aperture, 0.90). The scattered light was collected using backscatter geometry from a 25 μm pinhole and a holographic notch filter, dispersed using 2,400 lines/mm, and analyzed using a Peltier-cooled charge-coupled device detector composed of 256 × 1024 pixels (Andor Technology, Belfast, Ireland). Raman spectra were collected in six periods of 10 s each for point analysis. Spectra between 100 and 1,290 cm^{-1} were used to compare the spectra of calcium carbonate minerals (Parker et al., 2010; Wehrmeister et al., 2010).

3.3.2 SEM observation

The extent of diagenesis was determined using the PI, which was proposed for the evaluation of diagenetic alteration based on shell microstructure (Cochran et al., 2010; Knoll et al., 2016). First, the shell microstructure of a surface-etched polished slab coated with platinum was observed with SEM (SU6600; Hitachi High-Technologies, Tokyo, Japan) in the Laboratory of Geobiology at Nagoya University. Then, cracked shell surfaces coated with platinum were observed with SEM, and the preservation status was scored according to the PI (Cochran et al., 2010; Knoll et al., 2016).

3.4 Growth line analysis

Growth lines are observable as black-colored disconformities and translucent bands in accretionary-formed biogenic carbonates, which are caused by growth reduction or cessation. In bivalves, growth lines can be observed as concentric lines on the interior and exterior of the shells of various taxa; they were formed under environmental deterioration (e.g., tidal emersion and temperature extremes) or physical deterioration (Schöne et al., 2004; Schöne and Giere, 2005; de Winter et al., 2020). Growth lines tend to become darker with longer growth cessation. Growth lines act as records of the shell growth rate over various timescales (e.g., daily, fortnightly, and annually) (Kennish and Olsson, 1975; Ohno, 1989), indicating the timing of biological and environmental events (Kennish and Olsson, 1975; Sato, 1995). Therefore, growth lines can be used to elucidate organisms' growth strategies (Tanabe, 1988; Sugiura et al., 2014; Posenato et al., 2022).

Growth lines were observed on thin sections of each shell under crossed Nicol polarization and polished slabs of each shell under stereoscopic microscopy. To reduce diffuse reflections and obtain clear images, the surfaces of thin sections and polished slabs were immersed in water and then covered with a cover glass (Figure 4C). Enlarged images of thin sections and polished surfaces taken using microscopes were stitched into single TIFF images with Adobe Photoshop software (Adobe, San Jose, CA, USA). Throughout the study, growth lines in the outer shell layer were used for investigation because these growth lines can be observed more clearly than growth lines in the inner shell layer and hinge plate. To accurately distinguish the shell growth lines, the greyscale value of the shell cross-section was measured along the direction of shell growth, in accordance with the methods of Carré et al. (2005) and Otter et al. (2019). In fossil shells, black stains may appear in areas other than growth lines due to shell coloration or crack formation during fossilization. To remove background colors, the image of the polished section was first subjected to black and white conversion followed by a rolling ball algorithm (Sternberg, 1983) for background subtraction (10-pixel diameter). The width of growth increments (space between neighboring growth lines) was measured along the growth direction. All image processing operations were performed using ImageJ (https://imagej.nih.gov/ij/).

3.5 Stable isotope analysis

Carbonate powders (approximately 100 μg) were collected from the outer shell layers of polished shells along their growth direction using a drill bit 0.4 mm in diameter (Minitor Co., Ltd., Osaka, Japan). Stable oxygen and carbon isotope compositions of bivalve shells ($\delta^{18}O_{shell}$ and $\delta^{13}C_{shell}$, respectively) were measured with a Thermo Fisher Delta V Advantage isotope ratio mass spectrometer (Bremen, Germany) coupled to a ThermoQuest Kiel-III automated carbonate device (Bremen, Germany) at the Institute of Geology and Paleontology, Tohoku University, Sendai, Japan. Carbonate samples were reacted with 100% phosphoric acid at approximately 72°C. Both isotope ratios were expressed in conventional notation (δ, ‰) and calibrated to the NBS-19 international standard relative to Vienna Pee Dee Belemnite. The external precision (1σ) of the measured isotopic values was calculated based on repeated measurements of a laboratory reference sample (JCt-1) (Okai et al., 2004). The external precision (1σ) values of $\delta^{18}O_{shell}$ and $\delta^{13}C_{shell}$ were 0.05‰ and 0.03‰, respectively. Therefore, the error in seawater temperatures reconstructed based on the $\delta^{18}O_{shell}$ values measured in this study was approximately 0.9°C at the 95% significance level.

3.6 Paleotemperature estimation

Mollusks precipitate aragonite their shells at or near oxygen isotope equilibrium with ambient seawater (Epstein et al., 1953; Grossman and Ku, 1986; Watanabe and Oba, 1999). Seawater paleotemperature was estimated using the equation proposed by Grossman and Ku (1986) with a correlation adjustment of −0.27‰ (Dettman et al., 1999):

$$T(^\circ C) = 20.60 - 4.34\,(\delta^{18}O_{shell} - (\delta^{18}O_{seawater} - 0.27)) \quad (1)$$

where T represents seawater temperature, and $\delta^{18}O_{shell}$ and $\delta^{18}O_{seawater}$ represent oxygen isotope values of shell carbonates (relative to VPDB) and seawater where the bivalves were grown (relative to VSMOW), respectively. In this study, −1‰ was used for $\delta^{18}O_{seawater}$ according to the average $\delta^{18}O_{seawater}$ value of ocean water during the Late Cretaceous ice-free world (Shackleton and Kennett, 1975) and numerically simulated $\delta^{18}O_{seawater}$ values for the middle Cretaceous northwestern Pacific coastal region (Zhou et al., 2008). The validity of assuming a constant oxygen isotope ratio in the surrounding seawater is discussed in Section 5.3.

We reconstructed the monthly averaged paleotemperature of our study area from $\delta^{18}O_{shell}$ values using the algorithm developed by Judd et al. (2018). Input parameter values in our study are shown in Supplementary Table 1, but the following conditions were assumed when setting the parameters:

(1) The numbers of solar days within a fortnight cycle and one year were 14.7 and 365, respectively.

(2) The days of the year with the coldest and warmest temperatures (T_{pha}) within one year were regarded as January 1 and July 1, respectively, in all cases.

(3) The day of the year with maximum growth (G_{pha}) was regarded as the day in the middle of the fortnight cycle with the widest fortnightly growth increment.

We used younger age records of *C.* (*I.*) *delicatostriata* shells for the calculations because younger age records have paleotemperature and seasonal growth rate with sufficient time resolution.

4 Results

4.1 State of preservation

The studied shells showed no macro-scale diagenetic alterations in thin sections and polished sections (Figures 5A, B, E), aside from the presence of dark green needle-like chlorite in the outer part of the outer shell layer of *A. pseudoplana* (Figure 5E). These needle-like crystals extend perpendicular to the shell surface, and none straddle the growth lines.

The crossed-lamellar structure in the outer shell layer (Figure 5C) and complex crossed-lamellar structure in the inner shell layer (Figure 5D) were clearly observed in *C.* (*I.*) *delicatostriata* shells. In the *A. pseudoplana* shell, a crossed-acicular structure in the outer shell layer (Figure 5G), fine complex crossed-lamellar structures in the inner layer (Figure 5H), and irregular simple prismatic structures along the growth lines (Figure 5F) were preserved.

Raman spectroscopic analysis showed clear peaks at 153, 181, 206, 702, 706, and 1,085 cm^{-1} in all studied shells (Figure 6). The peaks at 153, 181, 206, 702, and 706 cm^{-1} together indicate the presence of aragonite (Parker et al., 2010); the peak at 1,085 cm^{-1} is the intrinsic Raman band of carbonate mineral (Wehrmeister et al., 2010). Considering that modern bivalves in the order Arcoida and the family Veneridae, which include *C.* (*I.*) *delicatostriata* and *A. pseudoplana*, respectively, produce aragonite shells (Kitamura, 2018), the two species also likely formed primarily aragonite shells. Therefore, the studied shells showed preservation of primary microstructure and mineralogy (aragonite) as indicated by SEM images and Raman spectroscopy (Figure 6).

In high-magnification SEM images, irregular thickness and fusions of crystals were observed in *C.* (*I.*) *delicatostriata* (Figures 7A–C). The PI of *C.* (*I.*) *delicatostriata* crossed-lamellar structures was 3 (good) for PU-1 (Figure 7A), 1 (poor) for PU-2 (Figure 7B), and 3 for PU-5 (Figure 7C) (Knoll et al., 2016). The PI of the *A. pseudoplana* shell could not be determined because the PI of the crossed-acicular structure has not been established (Figure 7D).

4.2 Growth line observation

Growth line visibility in the *C.* (*I.*) *delicatostriata* shell was compared between thin sections and polished sections of the same individuals (Figure 8). In the younger portion of the shells, growth lines of varying distinctness were clearly observed in both thin sections (Figure 8B) and polished sections (Figure 8D). Observation of polished sections under reflected light was more suitable for detecting faint growth lines than thin sections due to the brightness of the views. Near the ventral margin, prominent growth lines were observed in the thin sections (Figure 8C), while these lines were not clearly visible in the polished sections (Figure 8E). These results indicated that thin sections are suitable for observing growth lines throughout all ontogenetic stages, while polished sections are suitable for observing growth lines in younger portions of the shells. To monitor the shell growth pattern of *C.* (*I.*) *delicatostriata* throughout its lifetime, the most effective approach is to use thin sections and measure the width of the prominent growth increment along the growth direction.

The growth lines observed in thin sections and polished sections can be divided into two categories, prominent ("major") and faint ("minor") growth lines (Figures 5A, B, 9), according to their darkness. Major growth lines were darker than minor growth lines according to processed greyscale levels (Figure 9). The processed greyscale values more clearly reflected the blackness of growth lines than the raw greyscale values because the color inversion process and rolling ball algorithm subtracted background color heterogeneity (Figure 9). Notably, approximately 15 minor growth lines with low processed greyscale values were observed between neighboring major growth lines with high processed greyscale values in the polished sections (Figure 9).

10.3389/fmars.2024.1324436

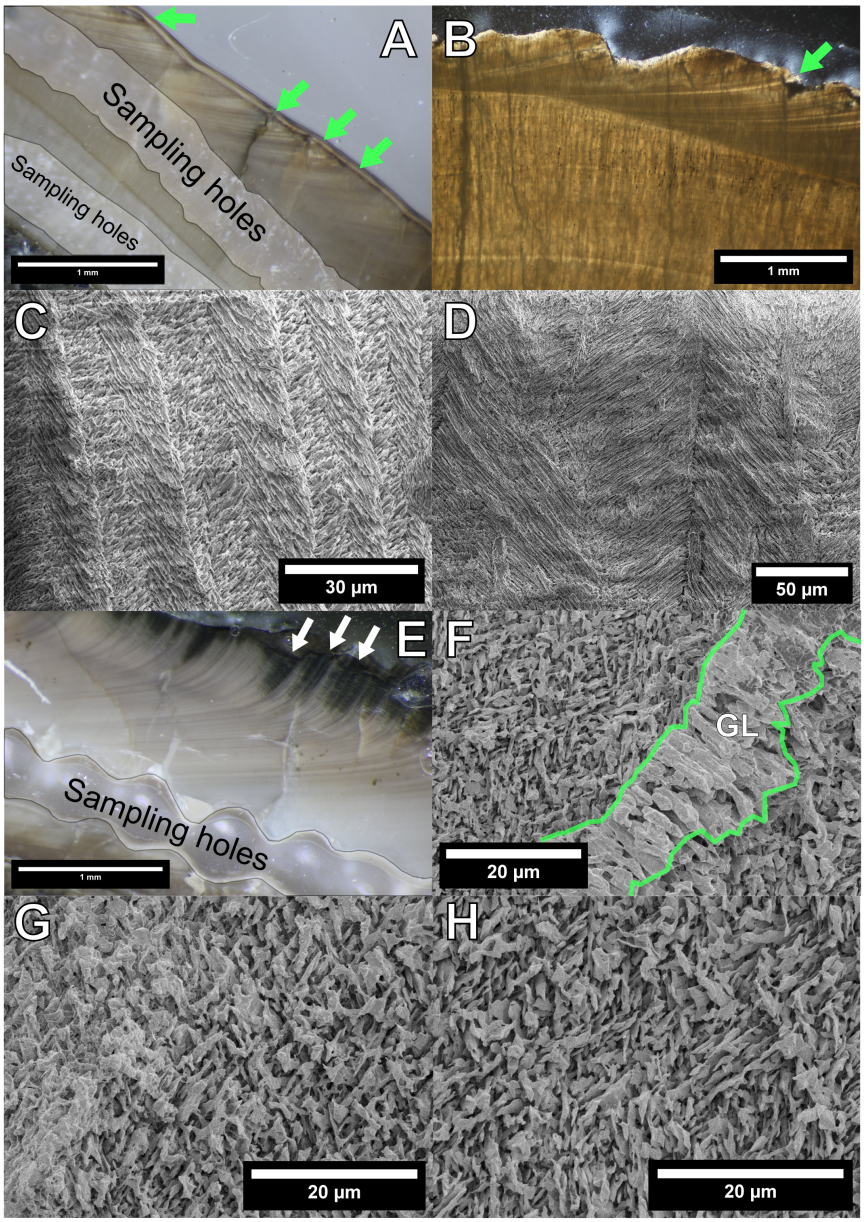

FIGURE 5
Polished section, thin section, and scanning electron microscopy (SEM) images of the studied mollusk materials. **(A)** Polished surface of *C.* (*I.*) *delicatostriata* (PU-1). **(B)** Thin section of *C.* (*I.*) *delicatostriata* (PU-2). Growth lines can be observed in both **(A, B)**. "Major" growth lines are indicated by light green arrows, and "minor" growth lines can be observed between each pair of "major" growth lines. **(C, D)** SEM images of *C.* (*I.*) *delicatostriata*. **(C)** Crossed-lamellar fabric in the outer shell layer. **(D)** Complex crossed-lamellar fabric in the inner shell layer. **(E)** Polished surface of *A. pseudoplana* showing clear growth lines. White arrows indicate chlorite-replaced parts. **(F–H)** SEM images of *A. pseudoplana*. **(F)** Irregular simple prismatic structures in the growth line (sandwiched between the light green lines); **(G)** crossed-acicular fabric in the OSL; and **(H)** fine complex crossed-lamellar fabric in the ISL.

4.3 Growth increment width

"Major" growth increment widths along the growth direction in thin sections of three *C.* (*I.*) *delicatostriata* shells are shown in Figure 10. The growth increment width varied among individuals due to intraspecific differences in growth rate and differences in the angles between the maximum growth direction and the cutting plane of each shell during thin section preparation.

4.4 $\delta^{18}O_{shell}$ and $\delta^{13}C_{shell}$ values

The $\delta^{18}O_{shell}$ profiles of the three *C.* (*I.*) *delicatostriata* shells (PU-1, 2, 5) and one *A. pseudoplana* shell showed clear cyclic variations of various amplitudes (Figure 10). The ranges of $\delta^{18}O_{shell}$ values were from −4.40‰ to −3.06‰ (average = −3.65‰, σ [standard deviation] = 0.40‰) for PU-1, from −5.12‰ to −3.31‰ (average = −4.38‰, σ = 0.43‰) for PU-2, from −5.33‰

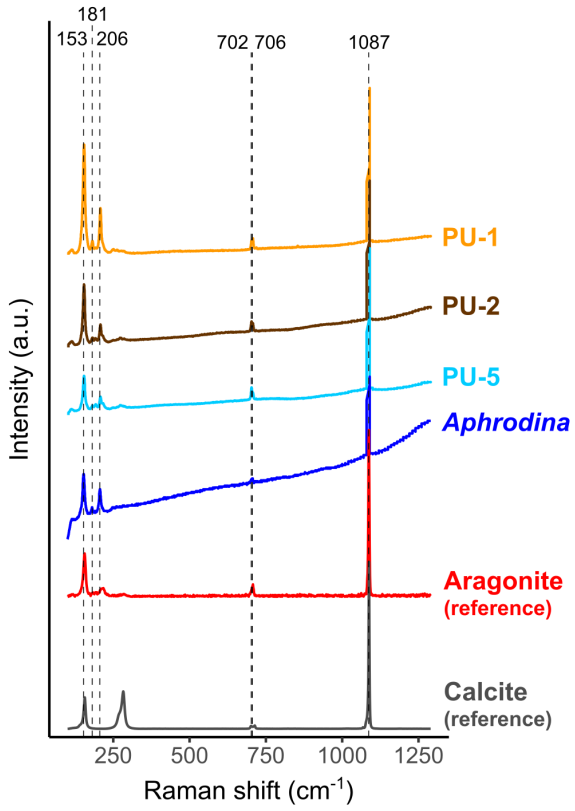

FIGURE 6
Raman spectra acquired at 100–1,290 cm^{-1} from the outer shell layer of all studied shells along with aragonite Raman spectra (aragonite R150021 with a 532 nm laser; red) and calcite Raman spectra (calcite R150075 with a 532 nm laser; gray) from RRUFF (rruff.info). Black dashed lines represent the positions of 153, 181, 206, 702, 706, and 1,085 cm^{-1}. Peaks at 153, 181, 206, 702, and 706 cm^{-1} indicate the presence of aragonite and the peak at 1,085 cm^{-1} indicates carbonate mineral.

to −2.93‰ (average = −3.70‰, σ = 0.39‰) for PU-5, and from −4.49‰ to −3.21‰ (average = −3.85‰, σ = 0.30‰) for *A. pseudoplana* (Table 1).

In contrast, the $\delta^{13}C_{shell}$ profiles of all analyzed shells did not show significant cyclicity compared with $\delta^{18}O_{shell}$ (Figure 10). The ranges of $\delta^{13}C_{shell}$ values were from −4.02‰ to 0.31‰ (average = −2.06‰, σ = 0.94‰) for PU-1, from −6.62‰ to −1.85‰ (average = −3.71‰, σ = 1.13‰) for PU-2, from −3.41‰ to −0.28‰ (average = −1.78‰, σ = 0.71‰) for PU-5, and from −2.59‰ to 0.48‰ (average = −0.78‰, σ = 0.54‰) for *A. pseudoplana* (Table 1).

5 Discussion

5.1 Evaluation of fossil preservation

5.1.1 State of preservation and shell microstructure

Shells composed primarily of aragonite are susceptible to diagenetic alteration and thus rarely retain their primary mineral composition and microstructure (Walliser et al., 2015; Posenato et al., 2022). With regard to the shell microstructure of *C.* (*I.*) *delicatostriata*, the crossed-lamellar structure in the outer shell layer (Figure 5C) and complex crossed-lamellar structure in the inner shell layer (Figure 5D) are same as those of *C. labiata*, an extant *Cucullaea* species (Taylor et al., 1969). The outermost part of the outer shell layer was absent although the shell was buried in a sandstone matrix (Figure 8C), indicating that the fossil shells were physically abraded or chemically dissolved before or during the fossilization process.

The *A. pseudoplana* shell showed a crossed-acicular structure in the outer shell layer (Figure 5G) and fine complex crossed-lamellar structure in the inner layer (Figure 5H). The needle-like crystals of chlorite present in the shell were considered pseudomorphs of biogenic aragonite produced by diagenetic alteration based on their morphology, distribution, and orientation. Silicification of biogenic carbonate with preserved microstructures has been observed in other areas (Suzuki et al., 1998; Zakhera et al., 2001; Foster et al., 2022). The arrangement of growth lines and crystals in the outermost part of the outer shell layer of *A. pseudoplana* is similar to some venerid bivalves (Chioninae and *Mercenaria stimpsoni*: Shimamoto, 1986); its shell microstructure is similar to the arcticid bivalve *Arctica islandica* (Dunca et al., 2009; Höche et al., 2021).

Dissolution traces and irregular crystal thickness were observed in high-magnification SEM images (Figure 7). A PI value of 3 was assigned for PU-1 and PU-5, whereas a value of 1 was assigned for PU-2; all of these values were lower than the best PI of 5 (classified as “excellent”; Cochran et al., 2010; Knoll et al., 2016), suggesting that the studied bivalves were affected by low-level diagenetic alteration. The partial chloritization of the surface of the *A. pseudoplana* shell is consistent with diagenetic alteration. However, chloritization of shell aragonite did not reach the parts used for stable isotope analysis in this study (Figure 5E).

The studied shells were buried in fine-grained sandstone. Biogenic carbonates in such coarse host rocks are considered highly susceptible to diagenetic alteration due to their high permeability and porosity. Nevertheless, the studied shells retained the initial shell microstructure and mineralogy although they had been slightly dissolved. The good state of preservation may be attributable to the well-cemented sandstone, which effectively limited pore water reaching the fossil sites. Well-preserved biogenic carbonate fossils buried in sediments with reduced influence of pore water are consistent with the finding that fossils of planktonic foraminifera in clay-rich sediments showed better preservation than such fossils in coarser-grained sediments (Pearson et al., 2001).

Yamamoto et al. (2017) reported a nonlinear relationship between the preservation of shell microstructure and geochemical composition, based on analyses of cathodoluminescence and SEM images, as well as measurements of the trace element concentrations and carbon and oxygen isotope compositions of Middle Pleistocene (approximately 0.8 Ma) brachiopod shells. They showed that the original isotopic composition was almost retained in many brachiopod shells that were altered due to meteoric diagenesis. Because there remains no robust criterion to assess diagenetic alteration, it is necessary to apply and cross-check multiple criteria. We suggest criteria that include assessment of whether

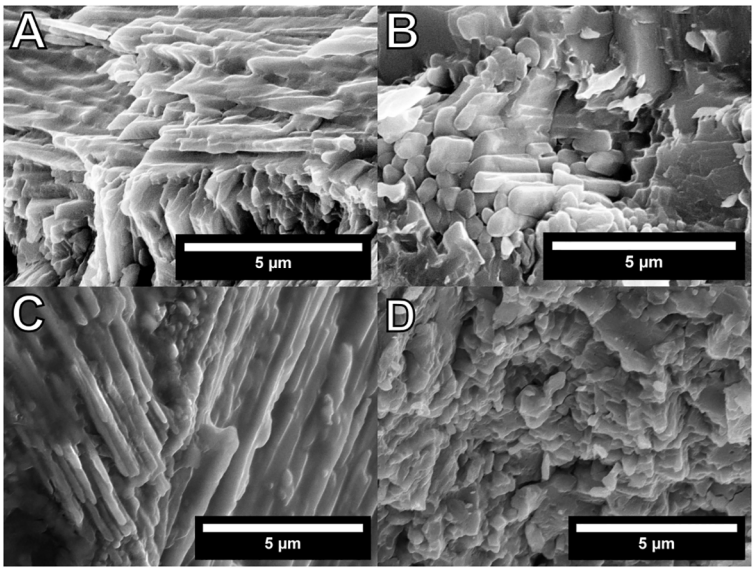

FIGURE 7
High-resolution images of the studied *Cucullaea* (*Idonearca*) *delicatostriata* (crossed-lamellar structure; PU-1, **A**; PU-2, **B**; PU-5, **C**) and *Aphrodina pseudoplana* (crossed-acicular structure; **D**) shells. Dissolution marks and irregular thickness of crystals can be observed in **(A–C)**. Preservation index values of 3 for PU-1, 1 for PU-2, and 3 for PU-5 were assigned. Indistinct structures can be observed in **(D)**, but the PI value could not be calculated because a PI for crossed-acicular structures has not been established.

the shells possess expected carbon and oxygen isotope compositions. Consequently, we concluded that the studied shells with PI of 3 retained their original carbon and oxygen isotope compositions.

5.1.2 Diagenetic effects on oxygen and carbon isotopes of the fossil shells

Previous studies suggested that geochemical and isotopic compositions of biogenic carbonate fossils with PI values > 3 are suitable as paleoenvironmental proxies (Cochran et al., 2010; Ryan et al., 2021; Tajika et al., 2023). The $\delta^{18}O_{shell}$ and $\delta^{13}C_{shell}$ values of PU-1 and PU-5, which have PI values of 3, were distributed in a similar area of the cross-plots (Figure 11). This similarity indicated that these shells have a similar preservation state and have not been affected by significant diagenetic alteration. Meanwhile, the $\delta^{18}O_{shell}$ and $\delta^{13}C_{shell}$ values of PU-2, with a low PI value of 1, were lower than the other shells (by approximately 1‰ and 2‰, respectively) (Figure 11). These results suggest that PU-2 was more diagenetically altered and affected to a greater extent by isotopic exchange of C and O between its shell aragonite and pore water with low $\delta^{18}O$ and $\delta^{13}C$ values. Pore water could supply lower $\delta^{18}O$ and $\delta^{13}C$ than contemporaneous seawater due to dissolution of decomposed organic matter (Cochran et al., 2010). Therefore, the isotopic records of PU-2 are excluded from further paleoenvironmental discussion due to diagenetic alteration. There is evidence from other areas that carbonate fossils strongly affected by diagenetic alteration have outlier $\delta^{18}O_{shell}$ and $\delta^{13}C_{shell}$ values compared with well-preserved fossils from the same locality (Cochran et al., 2010; Jones et al., 2022).

Although the isotopic composition of PU-2 was somewhat modified, its $\delta^{18}O$ values showed cyclicity similar to other studied shells (PU-1 and PU-5) with a better state of preservation, which may reflect seasonal environmental changes (Figure 10). Although Cochran et al. (2010) showed that stable isotope composition was modified in samples, they did not analyze isotopic composition along the growth axis or present any isotopic profiles. Given pristine shell microstructures, it is possible that variations in stable isotope composition, including seasonal variations, are preserved in shell carbonate even at low PI. Original seasonal $\delta^{18}O$ patterns can be preserved despite geochemical alteration. For example, heating can shift shell $\delta^{18}O$ values by 1.5‰, equivalent to 6°C–7°C in paleotemperature reconstruction, while the primary seasonal pattern is preserved (Moon et al., 2021). However, the stratigraphic horizon from which the studied shells were collected does not show any indications of exposure to high temperatures due to burial diagenesis or hydrothermal activity. Therefore, it is unlikely that the oxygen isotope profiles of the studied shells were shifted toward a smaller value while maintaining their initial seasonality.

5.2 Life history of *C.* (*I.*) *delicatostriata*

5.2.1 Timing of growth line formation in the shells of *C.* (*I.*) *delicatostriata*

The growth of carbonate shells (including bivalves) and skeletons is controlled by both tidal (Ohno, 1989; Schöne et al., 2003; Schöne and Giere, 2005) and daily rhythms (de Winter et al., 2023). In bivalves inhabiting tidally influenced areas, shell precipitation occurs during high tide; their growth is paused due to the stresses caused by tidal emersion and ebb currents during low tide, leading to the formation of growth lines (Evans, 1972; Ohno,

10.3389/fmars.2024.1324436

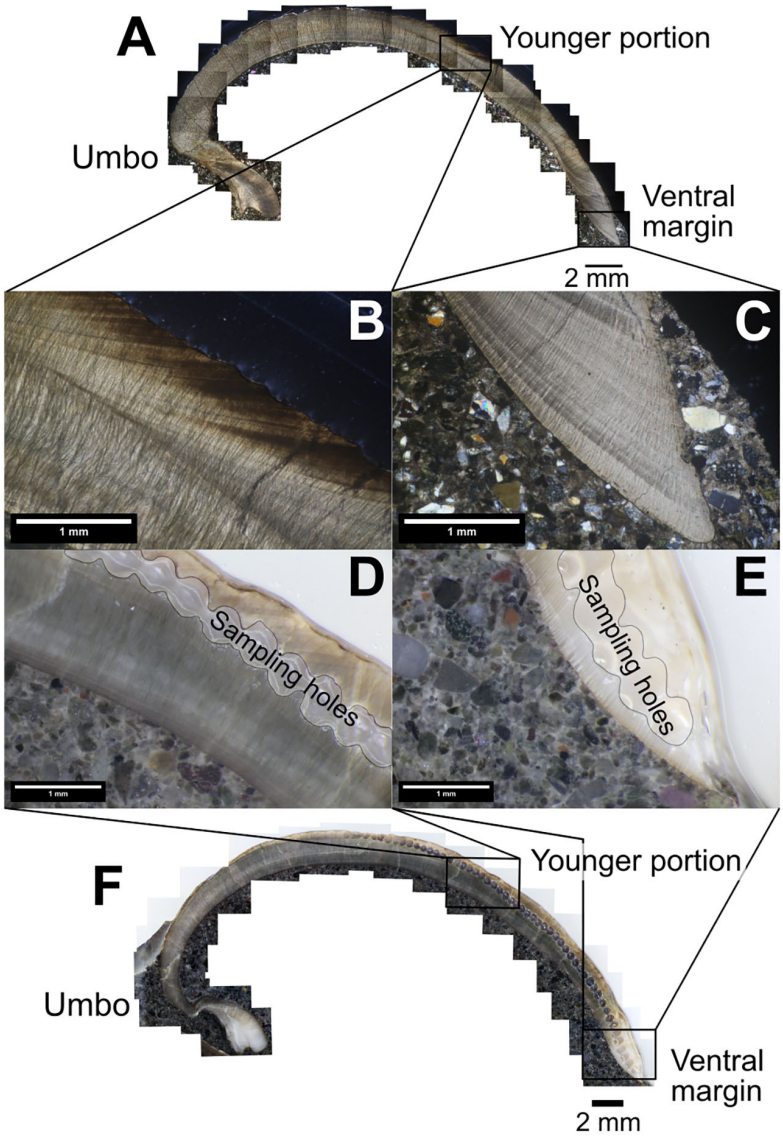

FIGURE 8
Comparison of growth line visibility in the outer shell layer between thin sections **(A–C)** and polished sections **(D–F)** of a *C.* (*I.*) *delicatostriata* shell (PU-5). The growth lines are clearly visible in the younger portions of both thin sections **(B)** and polished sections **(D)**. In the shell near the ventral margin, growth lines are clearly visible in the thin sections **(C)** but are indistinct in the polished sections **(E)**. Sampling holes in the polished sections **(D–F)** are the remains of samples taken for stable isotope analysis.

1989; Schöne et al., 2003; Reza Mirzaei et al., 2014). As tidal activity occurs twice per day, two growth lines are formed daily in the shells of bivalves inhabiting intertidal areas (Richardson, 1988; Ohno, 1989; Schöne et al., 2003). Bivalves in constantly immersed areas, such as subtidal zones, experience weaker tidal stresses and produce one growth line per day (Ohno, 1989; Reza Mirzaei et al., 2014). During spring tides, which occur on a fortnightly cycle (14.7 days), the stress at low tide is greater, which leads to more prominent growth line formation in both intertidal and subtidal bivalves (Azzoug et al., 2012; Reza Mirzaei et al., 2014). Irradiance (i.e., light intensity) is regarded as a major factor affecting bivalve shell formation controlled by daily rhythms (Ohno, 1989; Clark, 2005; Sano et al., 2012).

The most important consideration for establishing bivalve shell chronology from shell growth lines in geologic time is whether the environmental rhythms that drive modern shell growth line formation (i.e., tidal and daily rhythms) in the study periods were similar to today (Wierzbicki et al., 2023). The daily rhythm interval has lengthened at a rate of 1 s/5000 years on average (i.e., decreasing number of days per year) throughout geological time due to the decline in Earth's spin velocity (Darwin, 1880; Lantink et al., 2022). According to sclerochronological and geochemical analyses on rudist shells, day length was 23.5 h (372 days per year) in the Late Cretaceous (Campanian) (de Winter et al., 2020). The tidal rhythm in the middle Cretaceous was approximately similar to the present (14.8 days for semilunar month) because lunar-related

10.3389/fmars.2024.1324436

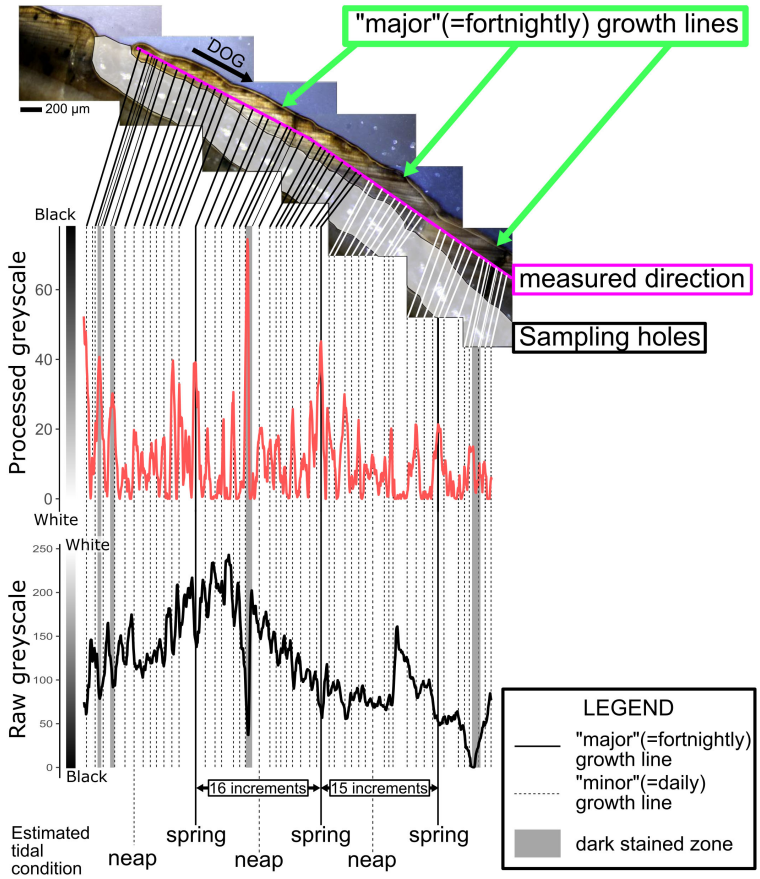

FIGURE 9
Polished section of the younger portion of a *C.* (*I.*) *delicatostriata* (PU-1) shell and greyscale values (raw and processed) along its growth direction in polished sections (pink line). Processed greyscale values were obtained by inverting the raw greyscale data and then applying the rolling ball algorithm. Raw greyscale data are shown as a black bold line and processed greyscale data are represented by red lines. Note that a high raw greyscale value is indicated by a light color, while a high processed greyscale value is represented by a dark color. The vertical black lines on the graph indicate the positions where growth lines were visually observed on the analyzed greyscale line. Solid lines indicate "major" growth lines and dashed lines indicate "minor" growth lines. The gray zones on the greyscale graph indicate the positions of dark staining. Numbers on the black arrows between lines represent the numbers of growth lines observed in the polished section. The estimated tidal condition (timing of spring tide and neap tide) is noted below the greyscale graphs.

rhythms, which are strongly related to tidal rhythm, were presumably more stable than solar rhythms throughout Earth's history (Williams, 2000; Bhattacharya and Jha, 2014; Wierzbicki et al., 2023). Calculations based on the above data indicated that the numbers of solar days, lunar days, and fortnightly growth lines per year during the middle Cretaceous were 372, 352.5, and 25.1, respectively. The numbers of growth lines according to solar days and lunar days per single fortnight cycle in the middle Cretaceous were 15.6 and 14.8, respectively.

Two different types of growth lines were recognized in the studied *C.* (*I.*) *delicatostriata* shells; specifically, distinct "major" and relatively indistinct "minor" growth lines were present, with an alternating pattern of a single "major" growth line followed by 15–16 "minor" growth lines (see Section 4.2) (Figure 9). The repeated appearance of prominent growth lines alternating with 15–16 faint growth lines can be explained as the "minor" growth lines corresponding to daily growth lines and "major" growth lines corresponding to fortnightly growth lines in modern bivalves (Carré et al., 2005; Azzoug et al., 2012). This character is consistent with the expected Cretaceous daily and fortnightly rhythm relations outlined above. Both "major" and "minor" growth lines presumably formed in response to tidal cycles; therefore, the growth lines of *C.* (*I.*) *delicatostriata* can be used for reliable inner shell chronology and as records of temporal shell growth.

5.2.2 Shell growth of *C.* (*I.*) *delicatostriata*

The $\delta^{18}O_{shell}$ values and growth lines of the studied shells can be used to delineate the life history of *C.* (*I.*) *delicatostriata*. The studied shells (PU-1, PU-2, and PU-5) exhibited distinct cyclicity of $\delta^{18}O_{shell}$ values, with an amplitude of approximately 1.5‰ over approximately 25 "major" (i.e., fortnightly) growth lines (Figure 10). Because the tidal cycle during the Cretaceous period was approximately similar to the present (Section 5.2.1 and Bhattacharya and Jha, 2014), the presence of approximately 25 fortnightly growth lines per year suggested that the bivalves continued to form shell carbonates throughout the year (Berry and Barker, 1968; Azzoug et al., 2012). The lowest and highest values of $\delta^{18}O_{shell}$ within these yearly growth line intervals represent

10.3389/fmars.2024.1324436

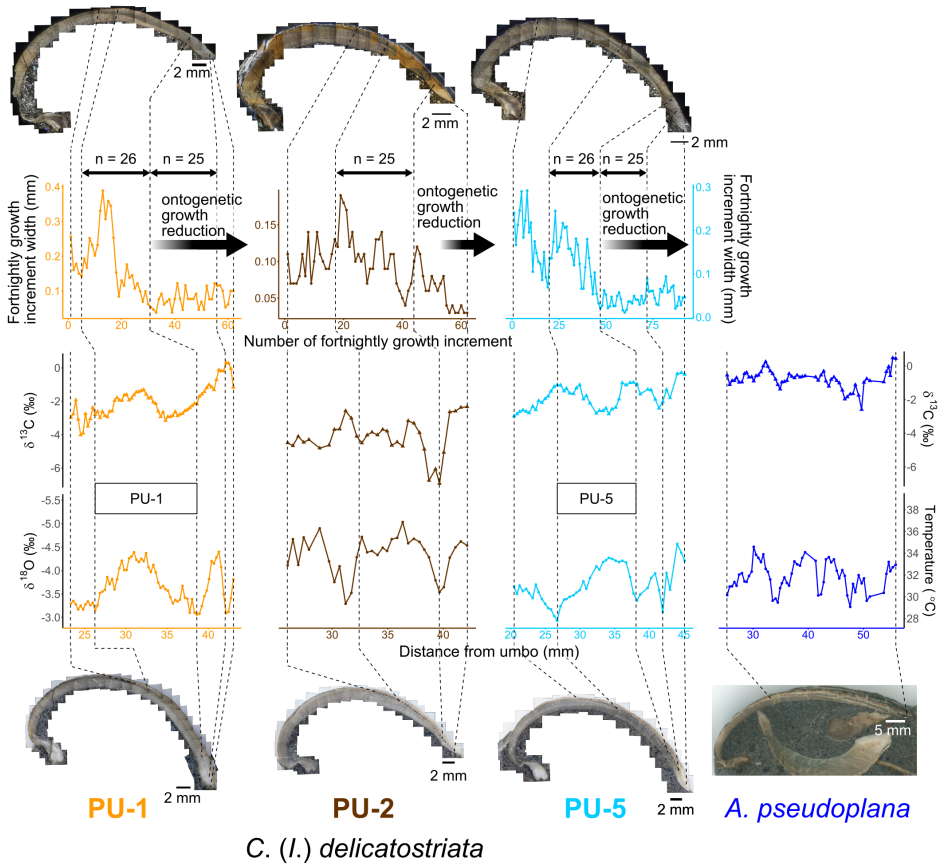

FIGURE 10
Fortnightly growth increment width of *C.* (*I.*) *delicatostriata*, $\delta^{18}O_{shell}$ and $\delta^{13}C_{shell}$ values of all studied shells with temperatures reconstructed based on Grossman and Ku (1986), and photographs of thin sections used for growth increment width measurement and polished slabs used for stable isotope analysis. Numbers above arrows indicate the number of growth lines between each pair of arrows. Approximately 25 lines are observed between the arrows, indicating a period of around 1 year. Bold black arrows on the graph of fortnightly growth increment width indicate periods of ontogenetic growth reduction. Squares on the graph of $\delta^{18}O_{shell}$ represent the positions of the annual growth increments used for monthly averaged paleotemperature calculations (Figure 13; Supplementary Table 2). For paleotemperature reconstruction from shell $\delta^{18}O$, a value of –1‰ was used for $\delta^{18}O_{seawater}$, obtained from Shackleton and Kennett (1975) and Zhou et al. (2008).

summer and winter values, respectively; the main factor controlling the $\delta^{18}O$ values is seawater temperature at the sites in which the shell grow. Therefore, the observed $\delta^{18}O_{shell}$ curves along the 25 fortnightly growth lines reflect seasonal seawater temperature variations. Bivalves that form their shell throughout the year typically inhabit the tropics (Thébault et al., 2007; Yamanashi et al., 2016) and submarine caves (Kitamura et al., 2012). Therefore, *C.* (*I.*) *delicatostriata* may have also inhabited an environment suitable for shell formation throughout the year (i.e., seasonal variation in seawater temperature).

The growth increment width and $\delta^{18}O_{shell}$ values of *C.* (*I.*) *delicatostriata* (top panels in Figure 10) represent temporal growth rate records. In younger portions of the shells, the fortnightly growth increment width shows an increase up to the maximum of 0.4 mm with a subsequent decrease (minimum = 0.05 mm) in 1 year, corresponding to 25 growth lines. The largest growth increment width was formed during the period spanning the $\delta^{18}O_{shell}$-based temperature minimum (winter) to its maximum (summer) (Figure 10), corresponding to the spring season. Conversely, the narrowest growth increments coincide with the coldest paleotemperatures and are regarded as representing winter (Figure 10). These observations suggest that the growth rate of *C.* (*I.*) *delicatostriata* reached its maximum in spring and minimum in winter. This growth pattern of bivalve shells is consistent with the patterns observed in extant bivalves inhabiting shallow-ocean areas and has been attributed to high spring phytoplankton abundance (Sato, 1997).

The "major" growth increment width and its variation significantly decreased toward the ventral shell margin (< 0.1 mm) (Figure 10), representing reductions in the shell growth rate and its seasonality during ontogeny. The presence of 25 "major" (i.e., fortnightly) growth increments within each annual growth cycle suggests that the shell was continuously precipitated throughout the year without any period of growth cessation. Although ontogenetic growth decline is common in modern bivalves (Jones and Quitmyer, 1996; Tanabe et al., 2017, 2020), ontogenetic growth characteristics in *C.* (*I.*) *delicatostriata*, which was continuous throughout the year associated with fortnightly (and daily) cycles, are similar to the characteristics of the extant tropical shallow-water bivalve *Tegillarca granosa* (Reza Mirzaei et al., 2017).

10.3389/fmars.2024.1324436

TABLE 1 Stable carbon and oxygen isotope values, paleotemperature estimated by Grossman and Ku (1986), and preservation status, as indicated by the preservation index (PI) according to Cochran et al. (2010) and Knoll et al. (2016), of the studied shells.

Bivalve taxon		*Cucullaea* (*Idonearca*) *delicatostriata*			*Aphrodina pseudoplana*
Shell name		PU-1	PU-2	PU-5	
PI score		3	1	3	undetermined
$\delta^{13}C_{shell}$ (‰)	Min	−4.02	−6.62	−3.41	−2.59
	Average	−2.06	−3.71	−1.78	−0.78
	Max	0.31	−1.85	−0.29	0.48
$\delta^{18}O_{shell}$ (‰)	Min	−4.40	−5.12	−4.57	−4.48
	Average	−3.65	−4.38	−3.70	−3.85
	Max	−3.06	−3.31	−2.93	−3.21
Temperature (°C)	Min	28.37	29.45	27.80	29.02
	Max	34.18	37.31	34.92	34.53
	Seasonal range	5.82	7.86	7.12	5.51
Number of samples		68	33	49	60

−1‰ was used as the $\delta^{18}O_{seawater}$ value.

5.3 Shallow-water temperature and its seasonality in the mid-latitude northwestern Pacific region during the Turonian

Based on the $\delta^{18}O_{shell}$ values of the two bivalve species and the relationships between temperature and aragonite $\delta^{18}O$ established by Grossman and Ku (1986; Equation 1), the annual shallow-water temperature in the middle Turonian Yezo Basin ranged from 27.8°C to 34.9°C (Figure 12; Table 1). Analysis of sedimentary facies suggested that *C.* (*I.*) *delicatostriata* and *A. pseudoplana* inhabited shallow depths less than some tens of meters (Ando and Kodama, 1998; Komatsu, 2013) (Figure 2). Because water temperature at these depths would not substantially differ from the temperature at the sea surface (Tanabe et al., 2017), the temperatures calculated in this study should reflect shallow-water temperature and its seasonality in the middle Turonian northwestern Pacific Ocean.

Seawater temperatures estimated from the shell $\delta^{18}O$ values and their seasonality can vary depending on assumed $\delta^{18}O_{seawater}$ values and their seasonal fluctuation at the site of shell growth. For example, for an actual $\delta^{18}O_{seawater}$ value 1‰ lower than the assumed value, the seawater temperature calculated based on the Equation 1 would increase by approximately 4°C. The $\delta^{18}O_{seawater}$ value varies depending on salinity because it increases with massive evaporation, whereas it decreases with strong precipitation and freshwater input due to ^{18}O depletion in the vapor and meteoric water (Craig, 1961). Based on the modern relationship of $\delta^{18}O_{seawater}$ and salinity, a salinity change of 1 causes a change of approximately 0.3‰ in $\delta^{18}O_{seawater}$ (Fairbanks et al., 1997; Abe et al., 2009; Takayanagi et al., 2015). Recent clumped isotope analysis of modern bivalve shells suggested

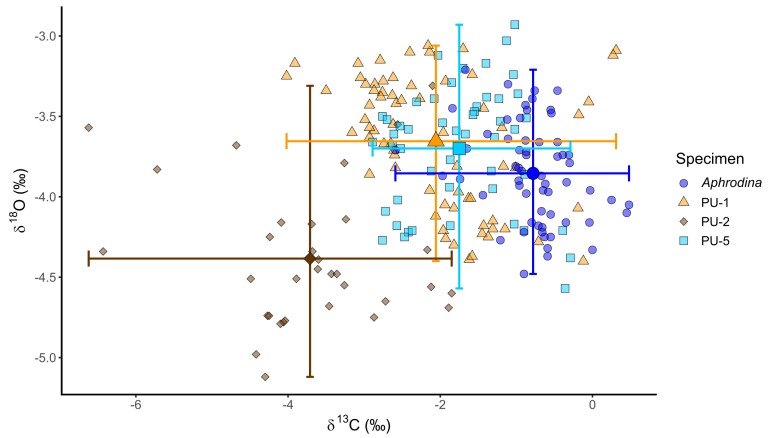

FIGURE 11
Cross-plots of $\delta^{18}O$ and $\delta^{13}C$ values of the studied *C.* (*I.*) *delicatostriata* (PU-1, 2, 5) and *A. pseudoplana* shells. Small translucent plots represent the original isotope values and large opaque plots show the average isotope ratio of each shell. Bars indicate the ranges of both isotope ratios for each shell.

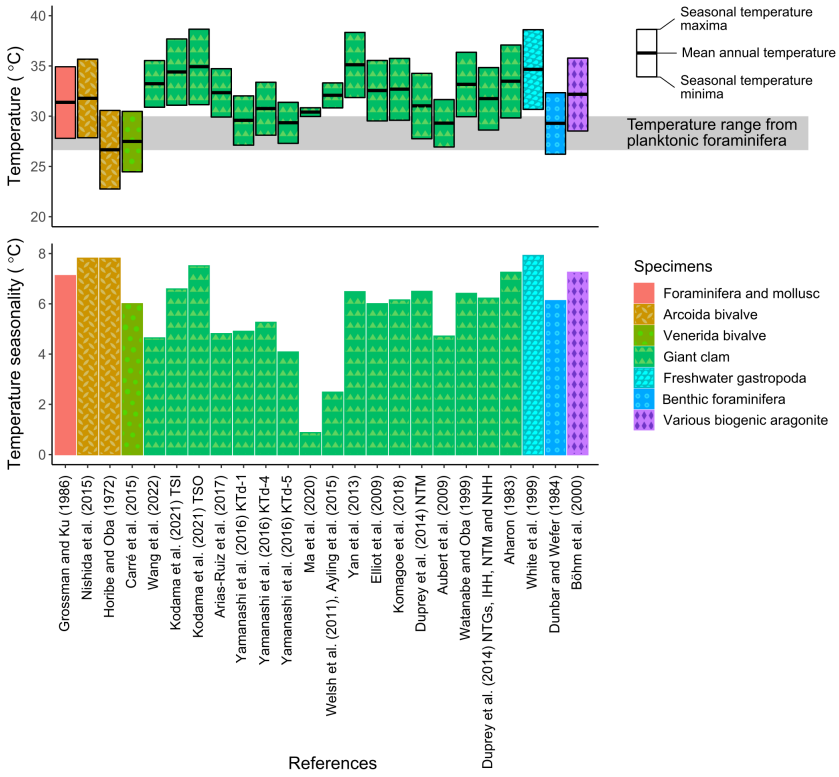

FIGURE 12
Comparison of shallow-water temperature and its seasonality calculated among various equations of temperature and aragonite $\delta^{18}O$. Aragonite $\delta^{18}O$ was derived from $\delta^{18}O_{shell}$ values of studied bivalve shells. TSI and TSO in Kodama et al. (2021), KTd-1, KTd-4, and KTd-5 in Yamanashi et al. (2016), and NTM, NTGs, IHH, and NHH in Duprey et al. (2014) represent the names of shells. Seasonal temperature maxima and minima were based on the maximum and minimum $\delta^{18}O_{shell}$ values of the studied shells. Mean annual temperature was calculated from monthly averaged $\delta^{18}O_{shell}$ values (Supplementary Table 2). The gray zone on the temperature plot represents the mean annual sea surface temperature (SST) of the middle–late Turonian Yezo Basin based on planktonic foraminiferal $\delta^{18}O$ (Moriya, 2011). The $\delta^{18}O_{seawater}$ value used for temperature estimation was –1.00‰.

that seasonal changes in $\delta^{18}O_{seawater}$ values make a significant contribution to those changes in $\delta^{18}O_{shell}$ values, thus affecting $\delta^{18}O_{shell}$-based seawater temperature estimates (Caldarescu et al., 2021). Furthermore, clumped isotope analyses of Cretaceous rudists and oysters revealed that $\delta^{18}O_{seawater}$ values at that time were not necessarily −1‰, which has been traditionally used for paleotemperature estimation from $\delta^{18}O$ values of biogenic carbonates during the Cretaceous in shallow oceans (de Winter et al., 2021; Jones et al., 2022). de Winter et al. (2021) also reported that large seasonal $\delta^{18}O_{seawater}$ fluctuations (approximately 1‰), which showed the highest values near the hottest season and lowest values near the coldest season, were present in the Campanian shallow ocean, resulting in underestimation of seawater temperature seasonality. However, it is difficult to assume that $\delta^{18}O_{seawater}$ changes over seasonal cycles.

The seasonal salinity ranges in the modern subtidal zone, especially at depths of more than 10 m, are small (salinity< 2) (Wanamaker et al., 2011; Kubota et al., 2017; Tanabe et al., 2017). This change corresponds to the $\delta^{18}O_{seawater}$ change of approximately 0.6‰, when converting salinity into $\delta^{18}O_{seawater}$; it may cause an error of< 3°C in reconstructing seawater temperatures (Grossman and Ku, 1986; Chauvaud et al., 2005). Therefore, some studies have assumed that seasonal $\delta^{18}O_{seawater}$ fluctuations were annually constant when reconstructing water temperature from $\delta^{18}O_{shell}$ values of bivalves inhabiting water with almost constant salinity (Wanamaker et al., 2011; Kubota et al., 2017; Tanabe et al., 2017). The studied species, *C.* (*I.*) *delicatostriata* and *A. pseudoplana*, presumably inhabited normal marine environments with limited freshwater influence because they are found in lower shoreface to inner shelf deposits, which likely formed at depths of 10 m to some tens of meters, and not in freshwater and estuary deposits such as oyster beds (Ando and Kodama, 1998; Komatsu, 2013) (Figure 2). The absence of neighboring prominent and faint growth lines in *C.* (*I.*) *delicatostriata* (Section 5.2.1 and Figure 9) also indicated that they did not live in the intertidal zone, which is commonly affected by freshwater input (Ohno, 1989; Tojo and Masuda, 1999; Miyaji et al., 2007; Reza Mirzaei et al., 2014). Massive freshwater inflow events, such as typhoons or heavy rains, may have occurred in the depositional area of the middle Turonian Mikasa Formation because of the humid climate conditions in the northwestern Pacific region, suggested by terrestrial organic $\delta^{13}C$ and numerical climate simulation, and the presence of HCS deposits (likely formed by storm events) in this formation (Ando, 1987; Hasegawa, 2003; Hasegawa et al., 2012; Higuchi et al., 2021). However, such short-term precipitation events are unlikely to be recorded in the $\delta^{18}O$ profiles of the studied shells due to their temporal resolution (more than one week), which is not sufficiently high for detection. Therefore, our seasonal $\delta^{18}O_{shell}$ variations likely

reflect shallow-water temperature seasonality at the time the shells inhabited.

The reconstructed paleotemperature in our study was consistent with shallow-water paleotemperature records (28°C–34°C) from the late Cenomanian mid-latitude (36°–45°N paleolatitude) North American Interior Seaway, derived from clumped isotope analysis on oyster fossil species (*Pycnodonte newberryi* shells from the Mancos Shale Formation at 36°N paleolatitude, *P. newberryi* shells from the Tropic Shale Formation at 37°N paleolatitude, *P. kellumi* shells from the Frontier Formation at 43°–45°N paleolatitude, and *P. kellumi* shells from the Greenhorn Formation at 44°N paleolatitude) using the temperature calculation formula of Petersen et al. (2019) (Jones et al., 2022). In contrast, planktonic foraminiferal $\delta^{18}O$ from the western extension of the Mikasa Formation indicated that the mean annual sea surface water temperature of the middle to late Turonian Yezo Basin ranged from 26°C to 29°C (Moriya, 2011). These temperatures are lower than temperatures determined from the studied shells (Figure 12). Such differences may have been due to variations in seawater temperatures during the Turonian and differences in growth site environments (e.g., depths) between benthic bivalves and planktonic foraminifera. Furthermore, the planktonic foraminiferal temperatures reported by Moriya (2011) do not necessarily reflect sea surface temperatures because planktonic foraminifera inhabit areas close to the sea surface and areas within the mixed layer. However, considering that Moriya (2011) did not provide detailed geological or paleontological data on the studied samples or information about the oxygen isotope thermometer used, it is not possible to identify the factors responsible for these discrepancies.

Differences in reconstructed temperatures between bivalves and foraminifera could have been partly due to differences in the equations representing the relationships between ($\delta^{18}O_{shell} - \delta^{18}O_{seawater}$) and seawater temperature (i.e., oxygen isotope thermometers). The equations proposed in previous studies differ among taxa and environmental settings (Nishida, 2020; Kodama et al., 2021). We calculated and compared shallow-water temperatures and their seasonality in the Turonian Yezo basin using 24 equations established for aragonite $\delta^{18}O$ in various modern marine calcifiers (Figure 12). These equations were derived from the arcid bivalve *Scapharca broughtonii* (Horibe and Oba, 1972; Nishida et al., 2015), venerid bivalve *Mesodesma donacium* (Carré et al., 2005), giant clam *Tridacna squamosa* (Arias-Ruiz et al., 2017; Kodama et al., 2021; Wang et al., 2022), *T. derasa* (Yamanashi et al., 2016), *T. gigas* (Elliot et al., 2009; Welsh et al., 2011; Yan et al., 2013; Ayling et al., 2015; Ma et al., 2020), *T. maxima* (Duprey et al., 2014; Komagoe et al., 2018), *Hippopus hippopus* (Watanabe and Oba, 1999; Aubert et al., 2009), a combination of giant clam species (Aharon, 1983; Duprey et al., 2014), the freshwater gastropod *Peregriana peregra* (White et al., 1999), various benthic foraminifera (Dunbar and Wefer, 1984), and various biogenic aragonites (Böhm et al., 2000).

Although the reconstructed seawater temperatures differed according to the equations used, they fell within a range from 22°C to 39°C, with seasonality of <8°C (Figure 12). In some cases (e.g., Dunbar and Wefer, 1984), the reconstructed temperatures were consistent with temperatures estimated from planktonic foraminifera for the same time period (Moriya, 2011), but more commonly, the reconstructed temperatures were higher than temperatures from planktonic foraminifera (e.g., Grossman and Ku, 1986 and Yan et al., 2013). The seawater temperatures reconstructed using equations derived from bivalves taxonomically close to *C.* (*I.*) *delicatostriata* (*Scapharca broughtonii*: Horibe and Oba, 1972) and *A. pseudoplana* (*Mesodesma donacium*: Carré et al., 2005) were slightly lower but roughly similar to temperatures derived from the studied bivalves, suggesting that the two fossil species precipitated their shells under physiological conditions similar to the conditions experienced by closely related extant species. The reconstructed seawater temperature of the middle Turonian Yezo Basin was significantly higher than the temperatures of the modern mid-latitude ocean (Figure 13). For example, the modern eastern Pacific Ishikari area of Hokkaido, Japan (44°N), has a surface seawater temperature of 4.8°C–22.1°C (monthly averaged data from Japan Meteorological Agency, 2024a). These findings suggest that extremely warm shallow water was present in the mid-latitude region during the middle Cretaceous "supergreenhouse" Earth.

Monthly averaged sub-annual scale $\delta^{18}O_{shell}$ data along the growth direction of two *C.* (*I.*) *delicatostriata* specimens (PU-1 and PU-5) (Figure 10) indicated that seasonal shallow-water temperature variation was approximately 6°C in the middle Turonian mid-latitude northwestern Pacific Ocean (Figure 13; Supplementary Table 2). This value is substantially smaller than temperature ranges in modern mid-latitude regions, such as Hokkaido, where the monthly averaged sea surface temperature changes by approximately 17°C throughout the year (Japan Meteorological Agency, 2024a) (Figure 13). Low seasonal variability of SST is typically observed in modern low-latitude tropical ocean areas, such as 22.7°C–29.3°C (6.6°C seasonality) derived from eastern Pacific data collected around southern Okinawa Island, the Ryukyu Islands, Japan (26°N; Japan Meteorological Agency, 2024b) (Figure 13). This finding is consistent with previous studies arguing that paleo-Hokkaido was located in a subtropical climate during the middle Cretaceous (e.g., Hay and Floegel, 2012).

5.4 Shallow-water temperatures during the Turonian greenhouse Earth

Shallow-water temperatures and their seasonal variations during the Turonian were estimated based on $\delta^{18}O_{shell}$ values (Figure 14) of rudist shells from the low-latitude Tethys Ocean (2–10 m water depth, < 30°N paleolatitude) in some previous studies. *Distefanella* sp. from the middle Turonian sediments in Zakynthos Island, Greece (91.1 Ma, 16.5°N paleolatitude) indicated one year seawater temperatures of 28.5°C–34.4°C with a seasonal variation of 5.9°C (Steuber et al., 2005). *Hippurites resectus* from the Gosau Group (the upper Turonian to the lower Coniacian, 89–91 Ma, 27.4°–27.5°N paleolatitude) and *Vaccinites inequicostatus* from the same group and Theresienstein, Austria, indicate seawater temperatures of 24.1°C–29.7°C (five years) and 25.9°C–35.0°C (1.5–2 years), respectively (Steuber et al., 2005; Walliser and Schöne, 2020). These temperatures were estimated using the equation of Anderson and Arthur (1983), assuming a constant $\delta^{18}O_{seawater}$ value of −1‰ throughout the year.

10.3389/fmars.2024.1324436

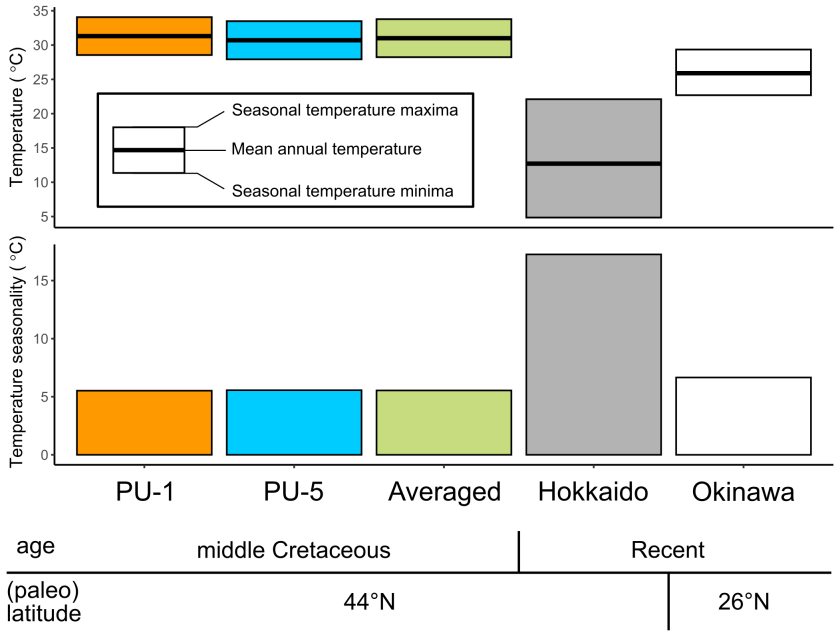

FIGURE 13
Comparison of monthly averaged shallow-ocean temperature and its seasonality in the western to northwestern Pacific regions among the middle Turonian, middle Cretaceous derived from this study (PU-1, PU-5, Averaged), and recent ocean derived from Japan Meteorological Agency (2024a) (Hokkaido) and Japan Meteorological Agency (2024b) (Okinawa). PU-1 and PU-5 refer to *Cucullaea* (*Idonearca*) *delicatostriata* shells examined in this study and averaged indicates averaged temperatures of PU-1 and PU-5. Mean annual temperature was calculated from monthly averaged temperature values (Supplementary Table 2).

The shallow-water temperature estimated in this study roughly coincided with the previous estimations; the common range was 28°C–35°C (Figure 14). One exception to this trend was the minimum temperature recorded in the Gosau Group (24.1°C), which was lower than the temperatures in the Mikasa Formation, although the Mikasa Formation was deposited in a higher latitude setting than the Gosau Group.

There are multiple possible explanations for the temperature differences outlined above, such as differences in $\delta^{18}O_{seawater}$ values between Tethys and Pacific Oceans. According to a numerical climate model of the global $\delta^{18}O_{seawater}$ value distributions, $\delta^{18}O_{seawater}$ values in the middle Cretaceous Tethys Ocean were approximately +0.5‰. This value is approximately 1.5‰ higher than the northwestern Pacific region at the same time (Zhou et al., 2008), as noted by Walliser and Schöne (2020). Consistent with the results of Zhou et al. (2008), the estimated shallow-water temperatures of the Gosau Group and Theresienstein depositional area were 31°C–43°C, higher than results for the Pacific derived in the present study. Warmer temperatures in the Tethys Ocean than the Pacific Ocean are consistent with planktonic foraminiferal biogeography of the middle Turonian Yezo Group with loss of frequent Tethyan type (tropical–subtropical) foraminifera and transitions to Transition type (warm–temperate) foraminifera bioprovinces (Nishi et al., 2003).

The effects of shallow-ocean currents can also explain the lower minimum seawater temperatures observed in the low-latitude Tethys Ocean (Walliser and Schöne, 2020) compared with the mid-latitude northwestern Pacific (this study). Cold currents flowed from the Arctic to the western Tethys Ocean, including the depositional area of the Gosau Group (Walliser and Schöne, 2020). In contrast, during the Turonian, the Pacific Ocean was separated from the Arctic Ocean by the Bering Land Bridge (Herman and Spicer, 1996, 2010; Herman et al., 2019). In this ocean–land configuration, the cold Arctic water could not flow into the Pacific Ocean, leading to warm shallow-water temperatures in the mid-latitude Pacific Ocean. The seasonal variations of shallow-water temperatures were commonly smaller than 7°C in the low-latitude Tethys (including the Gosau Group and Theresienstein area) and the mid-latitude Pacific (Figure 12).

Ivany (2012) noted that the seasonality of SST in the modern Northern Hemisphere is greatest at 40°–45°N. Our study site (44°N) exhibited good alignment with this maximal SST (or shallow-water temperature) seasonality zone of the Turonian Northern Hemisphere, indicating that maximum SST (or shallow-water temperature) seasonality in the mid-Cretaceous was similar to seasonality in the modern tropics. Additionally, the meridional temperature gradients and seasonal SST (or shallow-water temperature) ranges in the Northern Hemisphere were flatter and smaller in the mid-Cretaceous than at present. Low-temperature seasonality in the Northern Hemisphere during the Turonian is consistent with paleontological evidence from high-latitude plant and vertebrate fossils. Herman et al. (2019) reported conifer- and angiosperm-dominant floras from the Derevyannye Gory Formation (Turonian–Coniacian) of the New Siberia Island, Russia (70°N paleolatitude) and they concluded that low-temperature seasonality was present in the Turonian–Coniacian Arctic. Vandermark et al. (2007) reported that the extinct diapsid reptile *Champsosaurus* fossils from the Turonian–Coniacian sediments in Axel Heiberg Island, northern Canada (79°N, paleolatitude), was dominated by subadult-stage individuals, suggesting that temperatures suitable for

10.3389/fmars.2024.1324436

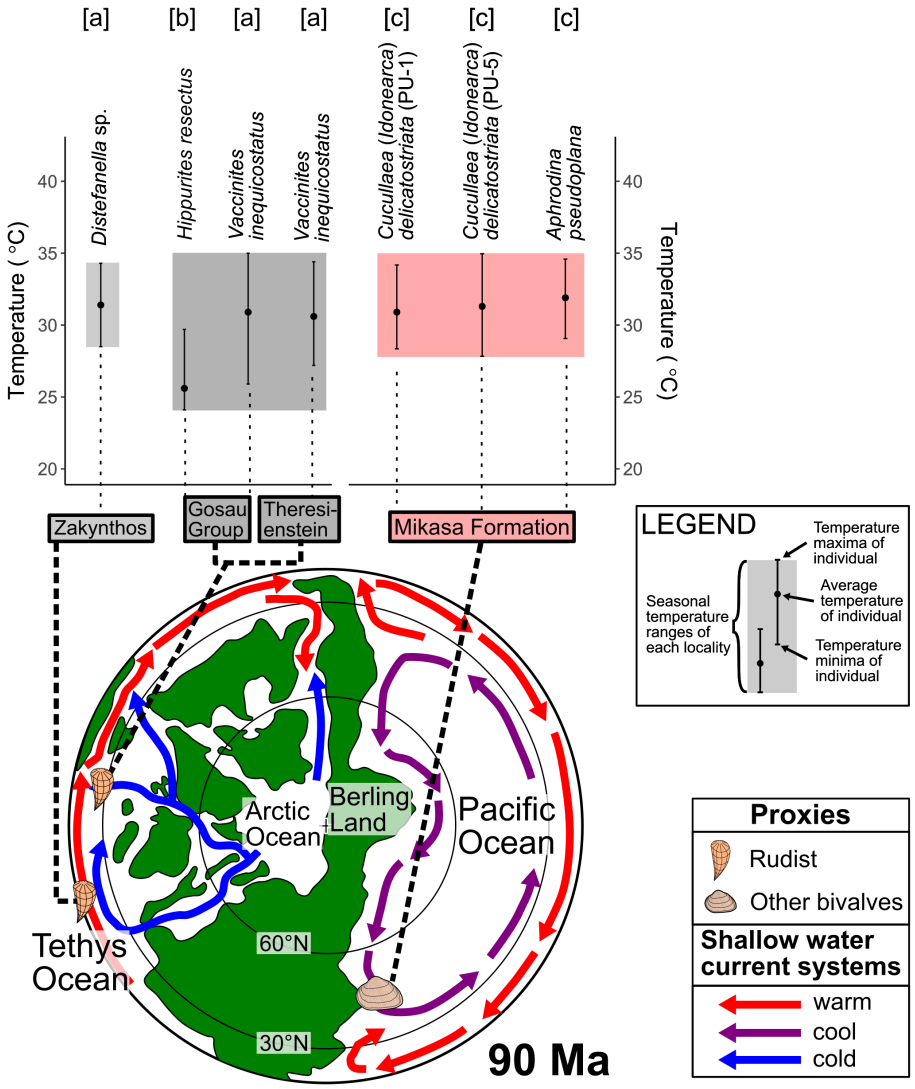

FIGURE 14
Shallow-water temperature records including seasonality during the Turonian compiled from this and previous studies ([a] Steuber et al. (2005); [b] Walliser and Schöne (2020); [c] this study), along with a paleogeographic map of the late Turonian (90 Ma) Northern Hemisphere modified from Nakajima et al. (2017) and Herman et al. (2019) with shallow-water current systems from Moiroud et al. (2013) and Mansour and Wagreich (2022). Shallow-water temperature data for individuals from the same region are grouped together as local shallow-water temperatures, with the Gosau Group and Theresienstein combined due to their close localities (Walliser and Schöne, 2020). The paleogeographic position of each locality is based on previous studies (Steuber et al., 2005; Walliser and Schöne, 2020) and paleomagnetic records for this study (Tamaki and Itoh, 2008). The $\delta^{18}O_{seawater}$ value for temperature estimation from shell carbonate $\delta^{18}O$ was –1.00‰ for all data according to the original article (Steuber et al., 2005; Walliser and Schöne, 2020).

reproduction and growth of reptiles were present during the Turonian–Coniacian at high latitudes due to a warm mean annual temperature with small temperature seasonality. The absence of ice sheets was presumably responsible for the reduced seasonal temperature variations on a global scale in the mid-Cretaceous (Steuber et al., 2005; Ivany, 2012). Under ice-free Earth conditions, the positive feedback of ice albedo becomes absent or is greatly weakened compared with today. In this case, the ice-free climate maintains warm shallow-water temperatures even in winter, resulting in slight temperature seasonality. Conversely, during the Eocene when the Antarctic ice sheet was ice-free, as in the Cretaceous, the annual SST range was greater than during the icehouse period in Antarctica (Buick and Ivany, 2004). There is a need for further data acquisition and numerical modeling of the latitudinal gradients and annual ranges of SST and air temperature during the middle Cretaceous and other greenhouse periods.

6 Conclusions

Growth increment and stable isotope analyses were performed on newly obtained bivalve fossils with preserved biogenic aragonite and shell microstructures from the middle Turonian Mikasa Formation, Yezo Group, in Hokkaido, Japan, to reveal the life history characteristics of the bivalves and sub-annual scale paleotemperature variations of mid-latitude shallow-water areas in the northwestern Pacific region during the Turonian. In *Cucullaea* (*Idonearca*) *delicatostriata*, approximately 25

fortnightly growth lines were observed per year, indicated by $\delta^{18}O_{shell}$, demonstrating that the annual cycles obtained from growth line analysis are consistent with those obtained from $\delta^{18}O_{shell}$ ratios. Growth increment width and $\delta^{18}O_{shell}$ values of *C.* (*I.*) *delicatostriata* revealed that they continuously produced their shells throughout the year, with the seasonal growth rate maximized in spring and minimized in winter. Reconstructed temperatures from bivalve $\delta^{18}O_{shell}$ values ranged from 28°C to 35°C and showed significantly smaller seasonality compared with temperatures in modern Hokkaido. The $\delta^{18}O_{seawater}$ value was assumed to be −1‰ without seasonal variations due to the limited influence of freshwater in the studied section. A comparison of temperature seasonality records with the same period from the Tethys Ocean showed similar values, indicating that tropical ocean conditions with low seasonality in mid-latitude regions were not limited to the Tethys Ocean but also occurred in the northwestern Pacific Ocean. Low shallow-water temperature seasonality in the mid-latitudes suggests that seasonal temperature fluctuations in the Northern Hemisphere were small in the middle Turonian "supergreenhouse" period.

Data availability statement

The original contributions presented in the study are included in the article/Supplementary Material. Further inquiries can be directed to the corresponding author.

Author contributions

SI: Writing – original draft, Conceptualization, Investigation, Methodology, Visualization, Data curation. HT: Investigation, Writing – review & editing, Data curation, Funding acquisition. YI: Writing – review & editing, Data curation, Funding acquisition. ST: Supervision, Writing – review & editing, Conceptualization, Funding acquisition. TO: Supervision, Writing – review & editing, Conceptualization, Funding acquisition, Investigation.

Funding

The author(s) declare financial support was received for the research, authorship, and/or publication of this article. This research was supported by Grant-in-Aid for Scientific Research (B: No. 19H02014 to TO, 23H01287to ST, 21K18642 and 23H01263 to YI).

Acknowledgments

We express our appreciation to the editor and three reviewers for their time and valuable comments. We would like to thank Y. Koketsu (Nagoya University) for assistant of Raman spectroscopic analysis. We also thank T. Miyaji (National Ainu Museum) for useful advice about growth line analysis. We gratefully acknowledge the Sorachi Forest Management Office for permitting us to conduct field survey. We thank S. Hayashi (Nagoya University) and Y. Ando (Mizunami Fossil Museum) for helping SEM observation. We also thank H. Oda (Tohoku University) for helping stable isotope analysis. We like to thank D. Nakai (Nagoya University) for advice about improving growth line observation. This work was partly supported by World Premier International Research Center Initiative (WPI), MEXT, Japan.

Conflict of interest

The authors declare that the research was conducted in the absence of any commercial or financial relationships that could be construed as a potential conflict of interest.

Publisher's note

Supplementary material

The Supplementary Material for this article can be found online at: https://www.frontiersin.org/articles/10.3389/fmars.2024.1324436/full#supplementary-material

References

Abe, O., Agata, S., Morimoto, M., Abe, M., Yoshimura, K., Hiyama, T., et al. (2009). A 6.5-year continuous record of sea surface salinity and seawater isotopic composition at Harbour of Ishigaki Island, southwest Japan. *Isotopes Environ. Health Stud.* 45, 247–258. doi: 10.1080/10256010903083847

Aharon, P. (1983). 140,000-yr isotope climatic record from raised coral reefs in New Guinea. *Nature* 304, 720–723. doi: 10.1038/304720a0

Anderson, T. F., and Arthur, M. A. (1983). Stable isotopes of oxygen and carbon and their application to sedimentologic and paleoenvironmental problems. *Stable Isot. Sediment. Geol.* 10, 1–151. doi: 10.2110/SCN.83.01.0000

Ando, H. (1987). Shallow marine deposits in the Mikasa Formation of the Middle Yezo Group in Central Hokkaido — with special reference to hummocky cross stratification. *Acad. Stud. Biol. Geol. Sch. Educ. Waseda Univ.* 36, 21–32. (in Japanese with English abstract)

Ando, H. (1990a). Shallow-marine sedimentary facies distribution and progradational sequences of the Mikasa Formation, Middle Yezo Group (Upper Cretaceous). *Jour. Geol. Soc Japan* 96, 453–469. doi: 10.5575/GEOSOC.96.453 (in Japanese with English abstract)

Ando, H. (1990b). Stratigraphy and shallow marine sedimentary facies of the Mikasa Formation, Middle Yezo Group (Upper Cretaceous). *Jour. Geol. Soc Japan* 96, 279–295_4. doi: 10.5575/GEOSOC.96.279 (in Japanese with English abstract)

Ando, H., and Kodama, T. (1998). Shallow-marine bivalvian faunal change during Cenomanian to Turonian, Late Cretaceous —Ponbetsu River section in the Mikasa Formation, Middle Yezo Group, Hokkaido, Japan—. *Bull. Mikasa City Museum* 2, 1–15. (in Japanese with English abstract)

Arias-Ruiz, C., Elliot, M., Bézos, A., Pedoja, K., Husson, L., Cahyarini, S. Y., et al. (2017). Geochemical fingerprints of climate variation and the extreme La Niña 2010–11 as recorded in a *Tridacna squamosa* shell from Sulawesi, Indonesia. *Palaeogeogr. Palaeoclimatol. Palaeoecol.* 487, 216–228. doi: 10.1016/J.PALAEO.2017.08.037

Aubert, A., Lazareth, C. E., Cabioch, G., Boucher, H., Yamada, T., Iryu, Y., et al. (2009). The tropical giant clam *Hippopus hippopus* shell, a new archive of environmental conditions as revealed by sclerochronological and $\delta^{18}O$ profiles. *Coral Reefs* 28, 989–998. doi: 10.1007/S00338-009-0538-0/FIGURES/7

Ayling, B. F., Chappell, J., Gagan, M. K., and McCulloch, M. T. (2015). ENSO variability during MIS 11 (424–374 ka) from *Tridacna gigas* at Huon Peninsula, Papua New Guinea. *Earth Planet. Sci. Lett.* 431, 236–246. doi: 10.1016/J.EPSL.2015.09.037

Azzoug, M., Carré, M., and Schauer, A. J. (2012). Reconstructing the duration of the West African Monsoon season from growth patterns and isotopic signals of shells of *Anadara senilis* (Saloum Delta, Senegal). *Palaeogeogr. Palaeoclimatol. Palaeoecol.* 346–347, 145–152. doi: 10.1016/J.PALAEO.2012.06.001

Barron, E. J. (1983). A warm, equable Cretaceous: The nature of the problem. *Earth Sci. Rev.* 19, 305–338. doi: 10.1016/0012-8252(83)90001-6

Beard, J. A., Ivany, L. C., and Runnegar, B. (2015). Gradients in seasonality and seawater oxygen isotopic composition along the early Permian Gondwanan coast, SE Australia. *Earth Planet. Sci. Lett.* 425, 219–231. doi: 10.1016/J.EPSL.2015.06.004

Berry, W. B. N., and Barker, R. M. (1968). Fossil Bivalve Shells indicate Longer Month and Year in Cretaceous than Present. *Nature* 217, 938–939. doi: 10.1038/217938b0

Bhattacharya, B., and Jha, S. (2014). Late cretaceous diurnal tidal system: A study from Nimar sandstone, Bagh group, Narmada Valley, Central India. *Curr. Sci.* 107, 1032–1037.

Böhm, F., Joachimski, M. M., Dullo, W. C., Eisenhauer, A., Lehnert, H., Reitner, J., et al. (2000). Oxygen isotope fractionation in marine aragonite of coralline sponges. *Geochim. Cosmochim. Acta* 64, 1695–1703. doi: 10.1016/S0016-7037(99)00408-1

Buick, D. P., and Ivany, L. C. (2004). 100 years in the dark: Extreme longevity of Eocene bivalves from Antarctica. *Geology* 32, 921–924. doi: 10.1130/G20796.1

Caldarescu, D. E., Sadatzki, H., Andersson, C., Schäfer, P., Fortunato, H., and Meckler, A. N. (2021). Clumped isotope thermometry in bivalve shells: A tool for reconstructing seasonal upwelling. *Geochim. Cosmochim. Acta* 294, 174–191. doi: 10.1016/J.GCA.2020.11.019

Carré, M., Bentaleb, I., Blamart, D., Ogle, N., Cardenas, F., Zevallos, S., et al. (2005). Stable isotopes and sclerochronology of the bivalve *Mesodesma donacium*: Potential application to Peruvian paleoceanographic reconstructions. *Palaeogeogr. Palaeoclimatol. Palaeoecol.* 228, 4–25. doi: 10.1016/J.PALAEO.2005.03.045

Chauvaud, L., Lorrain, A., Dunbar, R. B., Paulet, Y.-M., rard Thouzeau, G., ric Jean, F., et al. (2005). Shell of the Great Scallop *Pecten maximus* as a high-frequency archive of paleoenvironmental changes. *Geochemistry Geophys. Geosystems* 6. doi: 10.1029/2004GC000890

Clark, G. R. (2005). Daily growth lines in some living Pectens (Mollusca: Bivalvia), and some applications in a fossil relative: Time and tide will tell. *Palaeogeogr. Palaeoclimatol. Palaeoecol.* 228, 26–42. doi: 10.1016/j.palaeo.2005.03.044

Cochran, J. K., Kallenberg, K., Landman, N. H., Harries, P. J., Weinreb, D., Turekian, K. K., et al. (2010). Effect of diagenesis on the Sr, O, and C isotope composition of Late Cretaceous mollusks from the Western Interior Seaway of North America. *Am. J. Sci.* 310, 69–88. doi: 10.2475/02.2010.01

Craig, H. (1961). Isotopic variations in meteoric waters. *Sci.* 133, 1702–1703. doi: 10.1126/SCIENCE.133.3465.1702

Darwin, G. H. (1880). XX. On the secular changes in the elements of the orbit of a satellite revolving about a tidally distorted planet. *Philos. Trans. R. Soc London* 171, 713–891. doi: 10.1098/RSTL.1880.0020

Denton, G. H., Alley, R. B., Comer, G. C., and Broecker, W. S. (2005). The role of seasonality in abrupt climate change. *Quat. Sci. Rev.* 24, 1159–1182. doi: 10.1016/J.QUASCIREV.2004.12.002

Dettman, D. L., Reische, A. K., and Lohmann, K. C. (1999). Controls on the stable isotope composition of seasonal growth bands in aragonitic fresh-water bivalves (unionidae). *Geochim. Cosmochim. Acta* 63, 1049–1057. doi: 10.1016/S0016-7037(99)00020-4

de Winter, N. J., Goderis, S., Dehairs, F., Jagt, J. W. M., Fraaije, R. H. B., Van Malderen, S. J. M., et al. (2017). Tropical seasonality in the late Campanian (Late Cretaceous): Comparison between multiproxy records from three bivalve taxa from Oman. *Palaeogeogr. Palaeoclimatol. Palaeoecol.* 485, 740–760. doi: 10.1016/j.palaeo.2017.07.031

de Winter, N. J., Goderis, S., Van Malderen, S. J. M., Sinnesael, M., Vansteenberge, S., Snoeck, C., et al. (2020). Subdaily-scale chemical variability in a *Torreites sanchezi* rudist shell: implications for rudist paleobiology and the cretaceous day-night cycle. *Paleoceanogr. Paleoclimatol.* 35, e2019PA003723. doi: 10.1029/2019PA003723

de Winter, N. J., Killam, D., Fröhlich, L., De Nooijer, L., Boer, W., Schöne, B. R., et al. (2023). Ultradian rhythms in shell composition of photosymbiotic and non-photosymbiotic mollusks. *Biogeosciences* 20, 3027–3052. doi: 10.5194/bg-20-3027-2023

de Winter, N. J., Müller, I. A., Kocken, I. J., Thibault, N., Ullmann, C. V., Farnsworth, A., et al. (2021). Absolute seasonal temperature estimates from clumped isotopes in bivalve shells suggest warm and variable greenhouse climate. *Commun. Earth Environ.* 2, 1–8. doi: 10.1038/s43247-021-00193-9

Dunbar, R. B., and Wefer, G. (1984). Stable isotope fractionation in benthic foraminifera from the Peruvian continental margin. *Mar. Geol.* 59, 215–225. doi: 10.1016/0025-3227(84)90094-X

Dunca, E., Mutvei, H., Göransson, P., Mörth, C. M., Schöne, B. R., Whitehouse, M. J., et al. (2009). Using ocean quahog (*Arctica islandica*) shells to reconstruct palaeoenvironment in Öresund, Kattegat and Skagerrak, Sweden. *Int. J. Earth Sci.* 98, 3–17. doi: 10.1007/s00531-008-0348-6

Duprey, N., Lazareth, C. E., Dupouy, C., Butscher, J., Farman, R., Maes, C., et al. (2014). Calibration of seawater temperature and $\delta^{18}O$ seawater signals in *Tridacna maxima*'s $\delta^{18}O$ shell record based on in *situ* data. *Coral Reefs* 34, 437–450. doi: 10.1007/s00338-014-1245-z

Elliot, M., Welsh, K., Chilcott, C., McCulloch, M., Chappell, J., and Ayling, B. (2009). Profiles of trace elements and stable isotopes derived from giant long-lived *Tridacna gigas* bivalves: Potential applications in paleoclimate studies. *Palaeogeogr. Palaeoclimatol. Palaeoecol.* 280, 132–142. doi: 10.1016/J.PALAEO.2009.06.007

Epstein, S., Buchsbaum, R., Lowenstam, H. A., and Urey, H. C. (1953). Revised carbonate-water isotopic temperature scale. *Bull. Geol. Soc Am.* 54, 1315–1326. doi: 10.1130/0016-7606(1953)64[1315:RCITS]2.0.CO;2

Evans, J. W. (1972). Tidal growth increments in the cockle *Clinocardium nuttalli*. *Sci.* 176, 416–417. doi: 10.1126/SCIENCE.176.4033.416

Fairbanks, R. G., Evans, M. N., Rubenstone, J. L., Mortlock, R. A., Broad, K., Moore, M. D., et al. (1997). Evaluating climate indices and their geochemical proxies measured in corals. *Coral Reefs* 16, 93–100. doi: 10.1007/s003380050245

Foster, W. J., Hirtz, J. A., Farrell, C., Reistroffer, M., Twitchett, R. J., and Martindale, R. C. (2022). Bioindicators of severe ocean acidification are absent from the end-Permian mass extinction. *Sci. Rep.* 12, 1–9. doi: 10.1038/s41598-022-04991-9

Foster, G. L., Royer, D. L., and Lunt, D. J. (2017). Future climate forcing potentially without precedent in the last 420 million years. *Nat. Commun.* 8, 1–8. doi: 10.1038/ncomms14845

Grossman, E. L., and Ku, T. L. (1986). Oxygen and carbon isotope fractionation in biogenic aragonite: Temperature effects. *Chem. Geol. Isot. Geosci. Sect.* 59, 59–74. doi: 10.1016/0168-9622(86)90057-6

Hall, C. A., Dollase, W. A., and Corbató, C. E. (1974). Shell growth in Tivela stultorum (Mawe 1823) and *Callista chione* (Linnaeus 1758) (Bivalvia): annual periodicity, latitudinal differences, and diminution with age. *Palaeogeogr. Palaeoclimatol. Palaeoecol.* 15, 33–61. doi: 10.1016/0031-0182(74)90036-4

Hall, J. L. O., Newton, R. J., Witts, J. D., Francis, J. E., Hunter, S. J., Jamieson, R. A., et al. (2018). High benthic methane flux in low sulfate oceans: Evidence from carbon isotopes in Late Cretaceous Antarctic bivalves. *Earth Planet. Sci. Lett.* 497, 113–122. doi: 10.1016/J.EPSL.2018.06.014

Hasegawa, T. (2003). Cretaceous terrestrial paleoenvironments of northeastern Asia suggested from carbon isotope stratigraphy: Increased atmospheric pCO_2-induced climate. *J. Asian Earth Sci.* 21, 849–859. doi: 10.1016/S1367-9120(02)00109-8

Hasegawa, H., Tada, R., Jiang, X., Suganuma, Y., Imsamut, S., Charusiri, P., et al. (2012). Drastic shrinking of the Hadley circulation during the mid-Cretaceous Supergreenhouse. *Clim. Past* 8, 1323–1337. doi: 10.5194/cp-8-1323-2012

Hay, W. W. (2008). Evolving ideas about the Cretaceous climate and ocean circulation. *Cretac. Res.* 29, 725–753. doi: 10.1016/J.CRETRES.2008.05.025

Hay, W. W., and Floegel, S. (2012). New thoughts about the Cretaceous climate and oceans. *Earth-Science Rev.* 115, 262–272. doi: 10.1016/J.EARSCIREV.2012.09.008

Herman, A. B., Kostyleva, V. V., Nikolskii, P. A., Basilyan, A. E., and Kotel'nikov, A. E. (2019). New data on the Late Cretaceous flora of the New Siberia Island, New Siberian Islands. *Stratigr. Geol. Correl.* 27, 323–338. doi: 10.1134/S0869593819030031/FIGURES/7

Herman, A. B., and Spicer, R. A. (1996). Palaeobotanical evidence for a warm Cretaceous Arctic Ocean. *Nat. 1996 3806572* 380, 330–333. doi: 10.1038/380330a0

Herman, A. B., and Spicer, R. A. (2010). Mid-Cretaceous floras and climate of the Russian high Arctic (Novosibirsk Islands, Northern Yakutiya). *Palaeogeogr. Palaeoclimatol. Palaeoecol.* 295, 409–422. doi: 10.1016/J.PALAEO.2010.02.034

Higuchi, T., Abe-Ouchi, A., and Chan, W. (2021). Differences between present-day and cretaceous hydrological cycle responses to rising CO_2 concentration. *Geophys. Res. Lett.* 48, e2021GL094341. doi: 10.1029/2021GL094341

Hikida, Y., Suzuki, S., Togo, Y., and Ijiri, A. (2003). An exceptionally well-preserved fossil seep community from the Cretaceous Yezo Group in the Nakagawa area, Hokkaido, northern Japan. *Paleontol. Res.* 7, 329–342. doi: 10.2517/PRPSJ.7.329

Höche, N., Walliser, E. O., de Winter, N. J., Witbaard, R., and Schöne, B. R. (2021). Temperature-induced microstructural changes in shells of laboratory-grown *Arctica islandica* (Bivalvia). *PloS One* 16, e0247968. doi: 10.1371/JOURNAL.PONE.0247968

Horibe, S., and Oba, T. (1972). Temperature scales of aragonite-water and calcite-water systems. *Kaseki (Fossils)* 23, 69–74. (in Japanese with English abstract)

Hoşgör, İ., and Yılmaz, İ. (2019). Paleogeographic northeastern limits of *Aphrodina dutrugei* (Cocquand 1862)(Heterodonta, Bivalvia) from the Cenomanian of the Arabian Platform. *Riv. It. Paleontol. Strat.* 125, 421–431. doi: 10.13130/2039-4942/11773

Huber, B. T., Hodell, D. A., and Hamilton, C. P. (1995). Middle-Late Cretaceous climate of the southern high latitudes: stable isotopic evidence for minimal equator-to-pole thermal gradients. *Geol. Soc Am. Bull.* 107, 1164–1191. doi: 10.1130/0016-7606(1995)107<1164:MLCCOT>2.3.CO;2

Huber, B. T., MacLeod, K. G., Watkins, D. K., and Coffin, M. F. (2018). The rise and fall of the Cretaceous Hot Greenhouse climate. *Glob. Planet. Change* 167, 1–23. doi: 10.1016/j.gloplacha.2018.04.004

Huck, S., and Heimhofer, U. (2021). Early Cretaceous sea surface temperature evolution in subtropical shallow seas. *Sci. Rep.* 11, 1–9. doi: 10.1038/s41598-021-99094-2

Ivany, L. C. (2012). Reconstructing paleoseasonality from accretionary skeletal carbonates – challenges and opportunities. *Paleontol. Soc. Pap.* 18, 133–166.

Ivany, L. C., and Judd, E. J. (2022). Deciphering temperature seasonality in Earth's ancient oceans. *Annu. Rev. Earth Planet. Sci.* 50, 123–152. doi: 10.1146/annurev-earth-032320-095156

Japan Meteorological Agency (2024a) *Coastal sea-surface temperature information in coastal Ishikari area* (Hokkaido). Available online at: https://www.data.jma.go.jp/kaiyou/data/db/kaikyo/series/engan/engan109.html (Accessed 11, Mar, 2024).

Japan Meteorological Agency (2024b) *Coastal sea-surface temperature information in southern Okinawa island* (Ryukyu Islands). Available online at: https://www.data.jma.go.jp/kaiyou/data/db/kaikyo/series/engan/engan704.html (Accessed 11, Mar, 2024).

Jones, D. S. (1983). Sclerochronology: Reading the Record of the Molluscan Shell: Annual growth increments in the shells of bivalve molluscs record marine climatic changes and reveal surprising longevity. *Am. Sci.* 71, 384–391.

Jones, D. S., Arthur, M. A., and Allard, D. J. (1989). Sclerochronological records of temperature and growth from shells of *Mercenaria mercenaria* from Narragansett Bay, Rhode Island. *Mar. Biol.* 102, 225–234. doi: 10.1007/BF00428284

Jones, M. M., Petersen, S. V., and Curley, A. N. (2022). A tropically hot mid-Cretaceous North American Western Interior Seaway. *Geology* 50, 954–958. doi: 10.1130/G49998.1

Jones, D. S., and Quitmyer, I. R. (1996). Marking time with bivalve shells: oxygen isotopes and season of annual increment formation. *Palaios* 11, 340–346. doi: 10.2307/3515244

Judd, E. J., Wilkinson, B. H., and Ivany, L. C. (2018). The life and time of clams: Derivation of intra-annual growth rates from high-resolution oxygen isotope profiles. *Palaeogeogr. Palaeoclimatol. Palaeoecol.* 490, 70–83. doi: 10.1016/J.PALAEO.2017.09.034

Kennish, M. J., and Olsson, R. K. (1975). Effects of thermal discharges on the microstructural growth of *Mercenaria mercenaria*. *Environ. Geol.* 1, 41–64. doi: 10.1007/BF02426940

Kikuchi, K. (2018). The occurrence of *Paleodictyon* in shallow-marine deposits of the Upper Cretaceous Mikasa Formation, Hokkaido Island, northern Japan: Implications for spatiotemporal variation of the *Nereites* ichnofacies. *Palaeogeogr. Palaeoclimatol. Palaeoecol.* 503, 81–89. doi: 10.1016/J.PALAEO.2018.04.016

Kitagawa, Y., Takashima, R., and Itoh, Y. (2016). Paleomagnetism of the Sorachi and Yezo Group in the Ashibetsu area , central Hokkaido, Japan. *Bull. Tohoku Univ. Museum* 15, 109–125. (in Japanese with English abstract)

Kitamura, A. (2018). Combined sclerochronological and oxygen isotope analyses of marine bivalve shells to examine high-resolution Holocene environmental changes. *Quat. Res.* 57, 19–29. doi: 10.4116/jaqua.57.19 (in Japanese)

Kitamura, A., Yamamoto, N., and Kobayashi, K. (2012). Growth of the submarine cave-dwelling micro-bivalve *Carditella iejimensis*. *Venus (Japanese J. Malacol.* 70, 41–45. doi: 10.18941/venus.70.1-4_41

Knoll, K., Landman, N. H., Cochran, J. K., MacLeod, K. G., and Sessa, J. A. (2016). Microstructural preservation and the effects of diagenesis on the carbon and oxygen isotope composition of Late Cretaceous aragonitic mollusks from the Gulf Coastal Plain and the Western Interior Seaway. *Am. J. Sci.* 316, 591–613. doi: 10.2475/07.2016.01

Kodama, S., Takayanagi, H., Yoshii, K., Nhu Ha, T. T., Asami, R., Abe, O., et al. (2021). Carbon and oxygen isotope records of *Tridacna squamosa* shells from two different latitudes in the Ryukyu Islands. *Paleontol. Res.* 25, 79–92. doi: 10.2517/2020PR003

Komagoe, T., Watanabe, T., Shirai, K., Yamazaki, A., and Uematu, M. (2018). Geochemical and Microstructural Signals in Giant Clam *Tridacna maxima* Recorded Typhoon Events at Okinotori Island, Japan. *J. Geophys. Res. Biogeosciences* 123, 1460–1474. doi: 10.1029/2017JG004082

Komatsu, T. (2013). Palaeoecology of the mid-Cretaceous siphonate bivalve genus *Goshoraia* (Mollusca, Veneridae) from Japan. *Palaeontology* 56, 381–397. doi: 10.1111/J.1475-4983.2012.01206.X

Kubota, K., Shirai, K., Murakami-Sugihara, N., Seike, K., Hori, M., and Tanabe, K. (2017). Annual shell growth pattern of the Stimpson's hard clam *Mercenaria stimpsoni* as revealed by sclerochronological and oxygen stable isotope measurements. *Palaeogeogr. Palaeoclimatol. Palaeoecol.* 465, 307–315. doi: 10.1016/J.PALAEO.2016.05.016

Lantink, M. L., Davies, J. H. F. L., Ovtcharov, M., and Hilgen, F. J. (2022). Milankovitch cycles in banded iron formations constrain the Earth–Moon system 2.46 billion years ago. *EARTH Atmos. Planet. Sci.* 119, 1–10. doi: 10.1073/pnas.2117146119

Lidgard, S., and Crane, P. R. (1988). Quantitative analyses of the early angiosperm radiation. *Nature* 331, 344–346. doi: 10.1038/331344a0

Ma, X., Yan, H., Fei, H., Liu, C., Shi, G., Huang, E., et al. (2020). A high-resolution $\delta^{18}O$ record of modern *Tridacna gigas* bivalve and its paleoenvironmental implications. *Palaeogeogr. Palaeoclimatol. Palaeoecol.* 554, 109800. doi: 10.1016/J.PALAEO.2020.109800

MacLeod, K. G., Huber, B. T., Berrocoso, Á. J., and Wendler, I. (2013). A stable and hot Turonian without glacial $\delta^{18}O$ excursions is indicated by exquisitely preserved Tanzanian foraminifera. *Geology* 41, 1083–1086. doi: 10.1130/G34510.1

Maliva, R. G., Missimer, T. M., and Dickson, J. A. D. (2000). Skeletal aragonite neomorphism in Plio-Pleistocene sandy limestones and sandstones, Hollywood, Florida, USA. *Sediment. Geol.* 136, 147–154. doi: 10.1016/S0037-0738(00)00102-0

Mansour, A., and Wagreich, M. (2022). Earth system changes during the cooling greenhouse phase of the Late Cretaceous: Coniacian-Santonian OAE3 subevents and fundamental variations in organic carbon deposition. *Earth-Science Rev.* 229, 104022. doi: 10.1016/J.EARSCIREV.2022.104022

Marshall, D. J., and Burgess, S. C. (2015). Deconstructing environmental predictability: seasonality, environmental colour and the biogeography of marine life histories. *Ecol. Lett.* 18, 174–181. doi: 10.1111/ELE.12402

Matsumoto, T. (1951). The Yezo group and the Kwanmon group. *J. Geol. Soc Japan* 57, 95–98. doi: 10.5575/GEOSOC.57.95 (in Japanese)

Matsumoto, T. (1965). A monograph of the collignoniceratidae from Hokkaido part I: studies of the Cretaceous ammonites from Hokkaido and Saghalien-XIV. *Mem. Fac. Sci. Kyūsyū Univ. Ser. D Geol.* 16, 1–80. doi: 10.5109/1543624

Matsuno, K., Tanaka, K., and Mizuno, A. (1963). *Explainatory text of the geological map of Japan, Scale 1:50000* Vol. 179 (Iwamizawa: Geological Survey of Japan).

Meinshausen, M., Nicholls, Z. R. J., Lewis, J., Gidden, M. J., Vogel, E., Freund, M., et al. (2020). The shared socio-economic pathway (SSP) greenhouse gas concentrations and their extensions to 2500. *Geosci. Model. Dev.* 13, 3571–3605. doi: 10.5194/gmd-13-3571-2020

Meyer, K. W., Petersen, S. V., Lohmann, K. C., and Winkelstern, I. Z. (2018). Climate of the Late Cretaceous North American Gulf and Atlantic Coasts. *Cretac. Res.* 89, 160–173. doi: 10.1016/J.CRETRES.2018.03.017

Miyaji, T., Tanabe, K., and Schöne, B. R. (2007). Environmental controls on daily shell growth of *Phacosoma japonicum* (Bivalvia: Veneridae) from Japan. *Mar. Ecol. Prog. Ser.* 336, 141–150. doi: 10.3354/MEPS336141

Moiroud, M., Pucéat, E., Donnadieu, Y., Bayon, G., Moriya, K., Deconinck, J. F., et al. (2013). Evolution of the neodymium isotopic signature of neritic seawater on a northwestern Pacific margin: new constrains on possible end-members for the composition of deep-water masses in the Late Cretaceous ocean. *Chem. Geol.* 356, 160–170. doi: 10.1016/J.CHEMGEO.2013.08.008

Moon, L. R., Judd, E. J., Thomas, J., and Ivany, L. C. (2021). Out of the oven and into the fire: Unexpected preservation of the seasonal $\delta^{18}O$ cycle following heating experiments on shell carbonate. *Palaeogeogr. Palaeoclimatol. Palaeoecol.* 562, 110115. doi: 10.1016/J.PALAEO.2020.110115

Moriya, K. (2011). Development of the Cretaceous greenhouse climate and the oceanic thermal structure. *Paleontol. Res.* 15, 77–88. doi: 10.2517/1342-8144-15.2.077

Moriya, K., Wilson, P. A., Friedrich, O., Erbacher, J., and Kawahata, H. (2007). Testing for ice sheets during the mid-Cretaceous greenhouse using glassy foraminiferal calcite from the mid-Cenomanian tropics on Demerara Rise. *Geology* 35, 615–618. doi: 10.1130/G23589A.1

Nakajima, Y., Danilov, I. G., Hirayama, R., Sonoda, T., and Scheyer, T. M. (2017). Morphological and histological evidence for the oldest known softshell turtles from Japan. *J. Vertebr. Paleontol.* 37, e1278606. doi: 10.1080/02724634.2017.1278606

Nishi, H., Takashima, R., Hatsugai, T., Saito, T., Moriya, K., Ennyu, A., et al. (2003). Planktonic foraminiferal zonation in the Cretaceous Yezo Group, Central Hokkaido, Japan. *J. Asian Earth Sci.* 21, 867–886. doi: 10.1016/S1367-9120(02)00138-4

Nishida, K. (2020). Stable carbon and oxygen isotopes of molluscan shells: Implications to paleontological studies on biological carbonates. *Fossils* 107, 5–20. doi: 10.14825/kaseki.107.0_5 (in Japanese with English abstract)

Nishida, K., Suzuki, A., Isono, R., Hayashi, M., Watanabe, Y., Yamamoto, Y., et al. (2015). Thermal dependency of shell growth, microstructure, and stable isotopes in laboratory-reared *Scapharca broughtonii* (Mollusca: Bivalvia). *Geochemistry Geophys. Geosystems* 16, 2395–2408. doi: 10.1002/2014GC005634

Ohno, T. (1989). Variable rhythms of micro-growth striation formation in bivalve shells (Review). *Benthos Res.* 37, 35–48. doi: 10.5179/BENTHOS1981.1989.37_35 (in Japanese with English abstract)

Okai, T., Suzuki, A., Terashima, S., Inoue, M., Nohara, M., Kawahata, H., et al. (2004). Collaborative analysis of GSJ/AIST geochemieal reference materials JCp-1 (Coral) and JCt-1 (Giant Clam). *Chikyukagaku (Geochemistry)* 38, 281–286. doi: 10.14934/CHIKYUKAGAKU.38.281 (in Japanese with English abstract)

Otter, L. M., Agbaje, O. B. A., Kilburn, M. R., Lenz, C., Henry, H., Trimby, P., et al. (2019). Insights into architecture, growth dynamics, and biomineralization from pulsed Sr-labelled *Katelysia rhytiphora* shells (Mollusca, Bivalvia). *Biogeosciences* 16, 3439–3455. doi: 10.5194/BG-16-3439-2019

Parker, J. E., Thompson, S. P., Lennie, A. R., Potter, J., and Tang, C. C. (2010). A study of the aragonite-calcite transformation using Raman spectroscopy, synchrotron powder diffraction and scanning electron microscopy. *CrystEngComm* 12, 1590–1599. doi: 10.1039/B921487A

Pearson, P. N., Ditchfield, P. W., Singano, J., Harcourt-Brown, K. G., Nicholas, C. J., Olsson, R. K., et al. (2001). Warm tropical sea surface temperatures in the Late Cretaceous and Eocene epochs. *Nature* 413, 481–487. doi: 10.1038/35097000

Pederson, C., Mavromatis, V., Dietzel, M., Rollion-Bard, C., Nehrke, G., Jöns, N., et al. (2019). Diagenesis of mollusc aragonite and the role of fluid reservoirs. *Earth Planet. Sci. Lett.* 514, 130–142. doi: 10.1016/J.EPSL.2019.02.038

Petersen, S. V., Defliese, W. F., Saenger, C., Daëron, M., Huntington, K. W., John, C. M., et al. (2019). Effects of improved ^{17}O correction on interlaboratory agreement in clumped isotope calibrations, estimates of mineral-specific offsets, and temperature dependence of acid digestion fractionation. *Geochemistry Geophys. Geosystems* 20, 3495–3519. doi: 10.1029/2018GC008127

Petrizzo, M. R., Amaglio, G., Watkins, D. K., MacLeod, K. G., Huber, B. T., Hasegawa, T., et al. (2022). Biotic and paleoceanographic changes across the Late Cretaceous oceanic anoxic event 2 in the southern high latitudes (IODP sites U1513 and U1516, SE Indian Ocean). *Paleoceanogr. Paleoclimatol.* 37, e2022PA004474. doi: 10.1029/2022PA004474

Posenato, R., Crippa, G., de Winter, N. J., Frijia, G., and Kaskes, P. (2022). Microstructures and sclerochronology of exquisitely preserved Lower Jurassic lithiotid bivalves: Paleobiological and paleoclimatic significance. *Palaeogeogr. Palaeoclimatol. Palaeoecol.* 602, 111162. doi: 10.1016/J.PALAEO.2022.111162

Pucéat, E., Lécuyer, C., Donnadieu, Y., Naveau, P., Cappetta, H., Ramstein, G., et al. (2007). Fish tooth $\delta^{18}O$ revising Late Cretaceous meridional upper ocean water temperature gradients. *Geology* 35, 107–110. doi: 10.1130/G23103A.1

Reza Mirzaei, M., Hwai, A. T. S., and Khalil, M. (2017). Temporal Variation in Shell Growth Rate of Cockle *Anadara granosa* in Relation with its Reproductive Cycle. *J. Shellfish Res.* 36, 69–78. doi: 10.2983/035.036.0109

Reza Mirzaei, M., Yasin, Z., and Shau Hwai, A. T. (2014). Periodicity and shell microgrowth pattern formation in intertidal and subtidal areas using shell cross sections of the blood cockle, *Anadara granosa*. *Egypt. J. Aquat. Res.* 40, 459–468. doi: 10.1016/J.EJAR.2014.11.008

Richardson, C. A. (1988). Tidally produced growth bands in the subtidal bivalve *Spisula subtruncata* (Da Costa). *J. Molluscan Stud.* 54, 71–82. doi: 10.1093/MOLLUS/54.1.71

Ryan, D. R., Witts, J. D., and Landman, N. H. (2021). Palaeoecological analysis of a methane seep deposit from the Upper Cretaceous (Maastrichtian) of the U.S. Western Interior. *Lethaia* 54, 185–203. doi: 10.1111/let.12396

Sano, Y., Kobayashi, S., Shirai, K., Takahata, N., Matsumoto, K., Watanabe, T., et al. (2012). Past daily light cycle recorded in the strontium/calcium ratios of giant clam shells. *Nat. Commun.* 3, 761. doi: 10.1038/ncomms1763

Sato, S. (1995). Spawning periodicity and shell microgrowth patterns of the venerid bivalve *Phacosoma japonicum* (Reeve 1850). *Veliger* 38, 61–72. doi: 10.3800/PBR.2.77

Sato, S. (1997). Shell microgrowth patterns of bivalves reflecting seasonal change of phytoplankton abundance. *Paleontol. Res.* 1, 260–266. doi: 10.2517/prpsj.1.260

Schmitt, K. E., Huck, S., Krummacker, M., De Winter, N. J., Godet, A., Claeys, P., et al. (2022). Radiolitid rudists: an underestimated archive for Cretaceous climate reconstruction? *Lethaia* 55, 1–21. doi: 10.18261/let.55.4.4

Schöne, B. R., Dunca, E., Mutvei, H., and Norlund, U. (2004). A 217-year record of summer air temperature reconstructed from freshwater pearl mussels (*M. margarifitera*, Sweden). *Quat. Sci. Rev.* 23, 1803–1816. doi: 10.1016/J.QUASCIREV.2004.02.017

Schöne, B. R., Fiebig, J., Pfeiffer, M., Gleß, R., Hickson, J., Johnson, A. L. A., et al. (2005). Climate records from a bivalved Methuselah (*Arctica islandica*, Mollusca; Iceland). *Palaeogeogr. Palaeoclimatol. Palaeoecol.* 228, 130–148. doi: 10.1016/J.PALAEO.2005.03.049

Schöne, B. R., and Giere, O. (2005). Growth increments and stable isotope variation in shells of the deep-sea hydrothermal vent bivalve mollusk *Bathymodiolus brevior* from the North Fiji Basin, Pacific Ocean. *Deep Sea Res. Part I Oceanogr. Res. Pap.* 52, 1896–1910. doi: 10.1016/J.DSR.2005.06.003

Schöne, B. R., Tanabe, K., Dettman, D. L., and Sato, S. (2003). Environmental controls on shell growth rates and $\delta^{18}O$ of the shallow-marine bivalve mollusk *Phacosoma japonicum* in Japan. *Mar. Biol.* 142, 473–485. doi: 10.1007/s00227-002-0970-y

Shackleton, N. J., and Kennett, J. P. (1975). Paleotemperature history of the Cenozoic and the initiation of Antarctic glaciation: oxygen and carbon isotope analyses in DSDP Sites 277, 279 and 281. *Rep. Deep Sea Drill Pr* 29, 743–755. doi: 10.2973/dsdp.proc.29.117.1975

Shimamoto, M. (1986). Shell microstructure of the veneridae (Bivalvia) and its phylogenetic implications. *Sci. Rep. Tohoku Univ. Second Ser. Geol.* 56, 1–A40.

Shimizu, I., Tanaka, K., and Imai, I. (1955). *Explainatory text of the geological map of Japan, Scale 1:50000* (Kami-Ashibetsu: Geological Survey of Japan).

Squires, R. L. (2010). Northeast Pacific upper Cretaceous and paleocene glycymeridid bivalves. *J. Paleontol.* 84, 895–917. doi: 10.1666/09-130.1

Sternberg, S. R. (1983). Biomedical image processing. *Comput. (Long. Beach. Calif).* 16, 22–34. doi: 10.1109/MC.1983.1654163

Steuber, T., Rauch, M., Masse, J. P., Graaf, J., and Malkoč, M. (2005). Low-latitude seasonality of Cretaceous temperatures in warm and cold episodes. *Nat. 2005 4377063* 437, 1341–1344. doi: 10.1038/nature04096

Sugiura, D., Katayama, S., Sasa, S., and Sasaki, K. (2014). Age and growth of the ark shell *Scapharca broughtonii* (Bivalvia, arcidae) in Japanese waters. *J. Shellfish Res.* 33, 315–324. doi: 10.2983/035.033.0130

Suzuki, S., Togo, Y., and Hikida, Y. (1998). Preliminary report on the preservation of some molluscan fossils from Nakagawa-cho, Hokkaido, Japan. *Bull. Nakagawa Museum Nat. Hist.* 1, 81–94. (in Japanese with English abstract)

Tajika, A., Landman, N. H., Cochran, J. K., Nishida, K., Shirai, K., Ishimura, T., et al. (2023). Ammonoid extinction versus nautiloid survival: Is metabolism responsible? *Geology* 51 (7), 621–625. doi: 10.1130/G51116.1

Takashima, R., Kawabe, F., Nishi, H., Moriya, K., Wani, R., and Ando, H. (2004). Geology and stratigraphy of forearc basin sediments in Hokkaido, Japan: Cretaceous environmental events on the north-west Pacific margin. *Cretac. Res.* 25, 365–390. doi: 10.1016/J.CRETRES.2004.02.004

Takayanagi, H., Asami, R., Otake, T., Abe, O., Miyajima, T., Kitagawa, H., et al. (2015). Quantitative analysis of intraspecific variations in the carbon and oxygen isotope compositions of the modern cool-temperate brachiopod *Terebratulina crossei*. *Geochim. Cosmochim. Acta* 170, 301–320. doi: 10.1016/J.GCA.2015.08.006

Tamaki, M., and Itoh, Y. (2008). Tectonic implications of paleomagnetic data from upper Cretaceous sediments in the Oyubari area, central Hokkaido, Japan. *Isl. Arc* 17, 270–284. doi: 10.1111/J.1440-1738.2008.00617.X

Tamaki, M., Oshimbe, S., and Itoh, Y. (2008). A large latitudinal displacement of a part of Cretaceous forearc basin in Hokkaido, Japan: paleomagnetism of the Yezo Supergroup in the Urakawa area. *J. Geol. Soc Japan* 114, 207–217. doi: 10.5575/GEOSOC.114.207

Tanabe, K. (1988). An attempt for age estimation of bivalves using shell growth lines. *Benthos Res.* 32, 12–17. doi: 10.5179/BENTHOS1981.1988.12

Tanabe, K., Mimura, T., Miyaji, T., Shirai, K., Kubota, K., Murakami-Sugihara, N., et al. (2017). Interannual to decadal variability of summer sea surface temperature in the Sea of Okhotsk recorded in the shell growth history of Stimpson's hard clams (*Mercenaria stimpsoni*). *Glob. Planet. Change* 157, 35–47. doi: 10.1016/J.GLOPLACHA.2017.08.010

Tanabe, K., Miyaji, T., Murakami-Sugihara, N., Shirai, K., and Moriya, K. (2020). Annual shell growth patterns of three venerid bivalve mollusk species in the subtropical northwestern Pacific as revealed by sclerochronological and stable oxygen isotope analyses. *Mar. Biol.* 167, 1–15. doi: 10.1007/S00227-019-3637-7/FIGURES/8

Tashiro, M. (1979).). A STUDY OF THE "PENNATAE TRIGONIIDS" FROM JAPAN. *Trans. Proc. Paleontol. Soc Japan. New Ser.* 116, 179–222. doi: 10.14825/prpsj1951.1979.116_179

Tashiro, M. (1995). Stratigraphical occurrence of the Cenomanian bivalves from Hokkaido. *Mem. Fac. Sci. Kochi Univ. E Ser. Geol* 16, 15–31.

Taylor, J. D., Kennedy, W. J., and Hall, A. (1969). The shell structure and mineralogy of the Bivalvia. I. Introduction. Nuculacea-trigonacea. *Bull. Br. Museum (Natural Hist.) Zool* supplement, 1–125. doi: 10.5962/p.312694

Thébault, J., Chauvaud, L., Clavier, J., Guarini, J., Dunbar, R. B., Fichez, R., et al. (2007). Reconstruction of seasonal temperature variability in the tropical Pacific Ocean from the shell of the scallop, *Comptopallium radula*. *Geochim. Cosmochim. Acta* 71, 918–928. doi: 10.1016/J.GCA.2006.10.017

Tojo, B., and Masuda, F. (1999). Tidal growth patterns and growth curves of the Miocene potamidid gastropod *Vicarya yokoyamai*. *Paleontol. Res.* 3, 193–201. doi: 10.2517/prpsj.3.193

Vandermark, D., Tarduno, J. A., and Brinkman, D. B. (2007). A fossil champsosaur population from the high Arctic: Implications for Late Cretaceous paleotemperatures. *Palaeogeogr. Palaeoclimatol. Palaeoecol.* 248, 49–59. doi: 10.1016/J.PALAEO.2006.11.008

Vermeij, G. J. (1977). The Mesozoic marine revolution: evidence from snails, predators and grazers. *Paleobiology* 3, 245–258. doi: 10.1017/S0094837300005352

Walliser, E. O., and Schöne, B. R. (2020). Paleoceanography of the Late Cretaceous northwestern Tethys Ocean: Seasonal upwelling or steady thermocline? *PloS One* 15, e0238040. doi: 10.1371/JOURNAL.PONE.0238040

Walliser, E. O., Schöne, B. R., Tütken, T., Zirkel, J., Grimm, K. I., and Pross, J. (2015). The bivalve *Glycymeris planicostalis* as a high-resolution paleoclimate archive for the Rupelian (Early Oligocene) of central Europe. *Clim. Past* 11, 653–668. doi: 10.5194/cp-11-653-2015

Wanamaker, A. D., Kreutz, K. J., Schöne, B. R., and Introne, D. S. (2011). Gulf of Maine shells reveal changes in seawater temperature seasonality during the Medieval Climate Anomaly and the Little Ice Age. *Palaeogeogr. Palaeoclimatol. Palaeoecol.* 302, 43–51. doi: 10.1016/j.palaeo.2010.06.005

Wang, G., Yan, H., Liu, C., Han, T., Zhou, P., Zhao, N., et al. (2022). Oxygen isotope temperature calibrations for modern *Tridacna* shells in western Pacific. *Coral Reefs* 41, 113–130. doi: 10.1007/S00338-021-02208-5/TABLES/3

Watanabe, T., and Oba, T. (1999). Daily reconstruction of water temperature from oxygen isotopic ratios of a modern *Tridacna* shell using a freezing microtome sampling technique. *J. Geophys. Res. Ocean.* 104, 20667–20674. doi: 10.1029/1999JC900097

Wehrmeister, U., Soldati, A. L., Jacob, D. E., Häger, T., and Hofmeister, W. (2010). Raman spectroscopy of synthetic, geological and biological vaterite: a Raman spectroscopic study. *J. Raman Spectrosc.* 41, 193–201. doi: 10.1002/JRS.2438

Welsh, K., Elliot, M., Tudhope, A., Ayling, B., and Chappell, J. (2011). Giant bivalves (*Tridacna gigas*) as recorders of ENSO variability. *Earth Planet. Sci. Lett.* 307, 266–270. doi: 10.1016/J.EPSL.2011.05.032

White, R. M. P., Dennis, P. F., and Atkinson, T. C. (1999). Experimental calibration and field investigation of the oxygen isotopic fractionation between biogenic aragonite and water. *Rapid Commun. Mass Spectrom.* 13, 1242–1247. doi: 10.1002/(SICI)1097-0231(19990715)13:13

Wierzbicki, A., Wolfgring, E., Wagreich, M., Kędzierski, M., and Mertz-Kraus, R. (2023). Astronomically controlled deep-sea life in the Late Cretaceous reconstructed from ultra-high-resolution inoceramid shell archives. *Geobiology* 21, 474–490. doi: 10.1111/GBI.12548

Williams, G. E. (2000). Geological constraints on the Precambrian history of earth's rotation and the moon's orbit. *Rev. Geophys.* 38, 37–59. doi: 10.1029/1999RG900016

Yabe, H. (1926). A new scheme of the stratigraphical subdivision of the Cretaceous deposits of Hokkaidô. *Proc. Imp. Acad.* 2, 214–218. doi: 10.2183/PJAB1912.2.214

Yabumoto, Y., Hikida, Y., and Nishino, T. (2012). *Apsopelix miyazakii*, a new species of crossognathid fish (Teleostei) from the upper Cretaceous of Hokkaido, Japan. *Paleontol. Res.* 16, 37–46. doi: 10.2517/1342-8144-16.1.037

Yamamoto, K., Takizawa, M., Takayanagi, H., Asami, R., and Iryu, Y. (2017). Nonlinear relationship between preservation of microstructure and geochemical composition of Pleistocene brachiopod shells from the Ryukyu Islands, southwestern Japan. *Isl. Arc* 26, e12217. doi: 10.1111/iar.12217

Yamanashi, J., Takayanagi, H., Isaji, A., Asami, R., and Iryu, Y. (2016). Carbon and oxygen isotope records from *Tridacna derasa* shells: toward establishing a reliable proxy for sea surface environments. *PloS One* 11, e0157659. doi: 10.1371/JOURNAL.PONE.0157659

Yan, H., Shao, D., Wang, Y., and Sun, L. (2013). Sr/Ca profile of long-lived *Tridacna gigas* bivalves from South China Sea: A new high-resolution SST proxy. *Geochim. Cosmochim. Acta* 112, 52–65. doi: 10.1016/J.GCA.2013.03.007

Zakhera, M., Kassab, A., and Chinzei, K. (2001). *Hyotissocameleo*, a new Cretaceous oyster subgenus and its shell microstructure, from Wadi Tarfa, Easthern Desert of Egypt. *Paleontol. Res.* 5, 77–86. doi: 10.2517/prpsj.5.77

Zhou, J., Poulsen, C. J., Pollard, D., and White, T. S. (2008). Simulation of modern and middle Cretaceous marine $\delta^{18}O$ with an ocean-atmosphere general circulation model. *Paleoceanography* 23, PA3223. doi: 10.1029/2008PA001596